Low energy π^+ inelastic scattering from nuclei to the continuum

K. A. Aniol,* D. T. Chiang, K. G. R. Doss,† I. Halpern, M. Khandaker, D. W. Storm, and D. R. Tieger
University of Washington, Seattle, Washington 98195

P. D. Barnes, B. Bassalleck,‡ N. J. Colella, S. A. Dytman,§ R. A. Eisenstein,** R. Grace, C. Maher, D. Marlow,†† P. Pile,‡‡ R. Rieder, F. Takeutchi, and W. R. Wharton§§
Carnegie-Mellon University, Pittsburgh, Pennsylvania 15213

J. F. Amann
Los Alamos National Laboratory, Los Alamos, New Mexico 87545

J. Julien
Centre d'Etudes Nucléaires de Saclay, F-91191 Gif-sur-Yvette Cedex, France
(Received 22 April 1985)

Differential cross sections $d^2\sigma/d\Omega\,dE$ have been measured with a germanium telescope for the $(\pi^+,\pi^{+'})$ reaction on C, Ca, Sn, and Pb at incident energies of 67, 85, and 100 MeV. The yields at backward angles along with available information on total reaction cross sections are interpreted in terms of a simple classical model in which it is assumed that free-space pion nucleon interaction parameters prevail inside the nucleus. Among the experimental findings which can be accounted for in terms of the model (to within 10—15%) are the measured pion reaction cross sections and their dependence on target mass, the energy and mass dependences of the differential scattering cross section at backward angles, and the ratio of normal to charge exchange scattering cross sections. The model appears to overestimate the ratios π^- to π^+ reaction and scattering cross sections but there appear to be some inconsistencies in the available data.

I. INTRODUCTION

This paper reports on an experimental survey of the inclusive scattering of positive pions from nuclei at incident kinetic energies from 67 to 100 MeV. In these measurements, the energy spectra and angular distributions of scattered pions were obtained for a number of nuclei over virtually the full range of possible outgoing pion energies. Related earlier studies include the spectrum measurements of Burleson *et al.*,[1] of Rohlin *et al.*,[2] and of Blecher *et al.*[3] as well as the angular distribution studies of the Argonne group[4,5] and those of Ashery *et al.*[6]

The pion detector used in the present measurement was an intrinsic-germanium telescope. Those of its properties which mattered most for the present study are described in Sec. II.

The main results of our survey of $(\pi^+,\pi^{+'})$ scattering are reported in Sec. III where a number of representative pion spectra are displayed in a manner which allows them to be easily compared. Also shown are the angular distributions of the integrals over pion energy for the inelastic portions of the spectra. These distributions all show the strong backward peaking that is a well-known characteristic of pion scattering below the (3,3) resonance. Integrals of these angular distributions give the total inclusive inelastic scattering cross sections. These cross sections are recorded for several targets and incident energies in Table I.

In Sec. IV we give a simple classical description of the scattering based on the assumption that pion-nucleon scattering inside a nucleus is the same as it is outside. Models based on this viewpoint have long been a useful starting point for interpretations of observed particle emissions in medium and high energy reactions. Examples of their application to pion-induced reactions appear in the papers of Bertini,[7] Silbar,[8] Ingram,[9] Ginocchio,[10] Schiffer,[11] Fraenkel,[12] and others.[13]

Many of the earlier classical treatments take the form of cascade calculations in which the projectiles and their collision progeny are followed through the nucleus until they either escape or become part of the thermalized residual nucleus. The calculated distributions in yield, energy, and angle of emitted particles are then compared with experiment. Unfortunately, the parameter values and even the basic assumptions which enter into cascade calculations often come with considerable uncertainties. These tend to compound as the cascade is allowed to evolve through the nucleus. The present analysis suffers from some of these same difficulties. It differs however from other classical descriptions in that it concentrates exclusively on the very first interaction of the pion in the nucleus. This is possible for the pion because its interaction with nucleons has a number of very special features below the (3,3) resonance. (1) The pions are light and the backward portion of their c.m. angular distribution is therefore actually backward in the laboratory frame (unlike the situation in the collision of a nucleon or of a

heavier projectile with a stationary nucleon). This is important because the first pion-nucleon interaction generally occurs while the pion is still in the nuclear surface (see below). Thus backward scattered pions have short paths for escape and relatively little chance for second interactions. (2) The probability for such backward single scattering is enhanced below the (3,3) resonance by the fact that the pion-nucleon angular distribution actually happens to be backward peaked.[14] (3) The pion-nucleon cross section decreases rapidly with decreasing pion energy. This means that back-scattered pions have a good chance to escape without further interaction since these pions have much lower kinetic energy than the incident pions. (4) Pions are easily absorbed in nuclei. This severely reduces the probability that pions will scatter several times in the nucleus before they emerge. It helps reduce the ratio of multiple to single scattering. The ready absorption also means, of course, that there are no evaporated pions. (5) At these low incident energies there are also no secondary pions. On all of these counts one can expect the scattered pions to be mainly due to single scatterings in the nucleus.

An old but continuing question in the study of nuclear reactions concerns the difference between the interaction of a given projectile with a nucleon which is *inside* the nucleus from an equivalent collision when the nucleon is free. It would appear that the pion, as a projectile, can make unique contributions to this basic issue because it is possible to observe the pion after its first interaction in the nucleus with relatively little background from later stages in the cascade.

The classical model which we describe in Sec. IV is particularly simple because it is formulated in rather general terms. This permits us to include the most basic effects. We deal with a number of additional effects separately and where we are able to, we try to estimate the magnitudes of the changes which they would make to the calculated cross sections.

The use of the classical model allows one to separate to a considerable degree those features of the first collision which are reflections of the geometry of the pion-nucleus reaction from features which involve the nature of the interaction of the pion with nucleons. The model provides a framework which makes it easy to consistently compare the results of related measurements. Because of the multiplicity of small effects which can influence any particular cross section, predictions of this cross section which are based on some combination of these effects often remain unconvincing. It is generally more useful to compare various *sets* of related cross sections at the same time and it is for such comparisons that an explicit geometrical model is of great help.

The main observational features which are connected to the first pion interaction in the nucleus are (1) the total reaction cross section and (2) the 180° differential scattering cross section. Model calculations for these cross sections are compared with data in Secs. V and VI, respectively.

We find that a number of basic features of measured pion-nucleus cross sections can be accounted for on a level of 10% to 15% in terms of the model. These include the magnitudes and the dependence on target mass of the reaction cross sections and the energy dependence of the differential scattering cross sections as well as the ratio of normal to charge exchange scattering. The model overestimates the measured ratios of corresponding π^- to π^+ cross sections but there appear to be some inconsistencies in the relevant data.

II. EXPERIMENTAL PROCEDURES

A. Arrangement of the apparatus

Inelastic spectra for $(\pi^+,\pi^{+'})$ were obtained with an intrinsic Ge telescope at angles between 40° to 152° for a number of targets at incident energies from 67 to 100 MeV. Although not all of the targets were measured at all angles and incident energies, enough spectra were measured to define the A dependences, angular distributions, and energy dependences of the cross sections. The general arrangement of the apparatus is shown in Fig. 1. We take up the elements shown in the figure in order, with emphasis on those features which gave rise to special problems and those that had a special bearing on the final results.

1. Beam characteristics

The experiment was carried out at the low energy pion channel (LEP) at the Los Alamos Meson Physics Facility (LAMPF) with an incident pion flux of 10^7 to 10^8 pions per second. The channel momentum acceptance $\Delta P/P$ (FWHM) was typically set at 1 to 2 percent.

The beam provided by the channel contains, in addition to the pions, a considerable number of muons and elec-

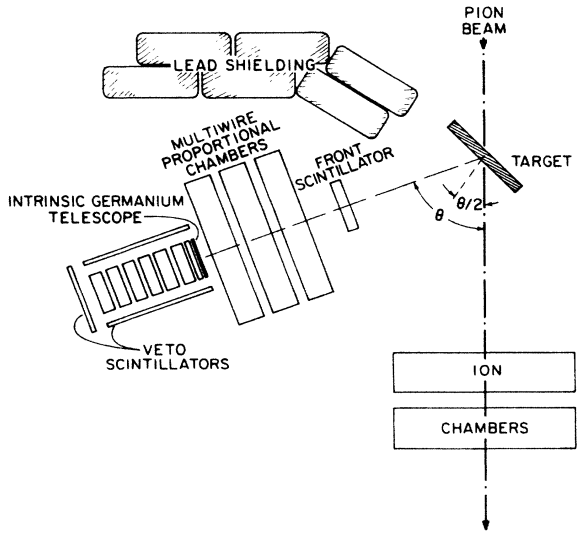

FIG. 1. The arrangement of the experimental apparatus (not to scale).

trons with the same momentum as the pions. Muons are also produced from the decay of pions immediately upstream from the target. (Protons in the beam were removed by an absorber in the middle of the channel.) The muons and electrons gave rise to backgrounds in both the beam monitor (a redundant pair of ion chambers placed in series downstream from the target) and in the detector of scattered pions. To calibrate the ion chambers, the scattering of pions from hydrogen in a polyethylene target was measured. Using the well-known πp cross section,[14] the calibration comes out in terms of the flux of pions only. The elimination of background in the pion detector from Coulomb-scattered and decay muons and electrons was especially troublesome at forward angles. It is discussed below.

Before undertaking the present measurements, it was necessary to establish an upper limit for still another possible beam contaminant, namely degraded pions. Such pions would elastically scatter in a target (with cross sections large compared to inelastic cross sections) and they would be indistinguishable from genuine inelastic scatterings. A large ratio of degraded to undegraded pions in the beam would have made the present experiment unfeasible. With the detector positioned at zero degrees, it was however established that the low energy tail in the pion spectrum was small enough so that even at the most forward angles the possible contamination of the observed inelastic spectra by degraded pions did not exceed 10%. At backward angles, the limit was much smaller.

2. Targets

The targets reported in the present paper include carbon, calcium, tin, and lead. A number of additional targets were examined at some angles and energies and the results for these targets were found to interpolate reasonably with those for the primary targets.

The position of the targets was about 1.3 m from the channel exit. Here the beam spot size was typically 3 cm vertically and 5 cm horizontally. Target thicknesses varied from $\simeq\frac{1}{3}$ g/cm^2 for light nuclei to $\simeq$2 g/cm^2 for heavy nuclei corresponding to pion energy losses of up to 6 MeV and to energy straggling of up to 2 MeV. This amount of resolution loss roughly matched that arising from the large momentum acceptance of the channel. For runs at the most backward angles, the targets were oriented in reflection rather than in transmission geometry. To maintain an acceptable energy spread, it was necessary to make the reflection targets substantially thinner than the transmission targets. Fortunately, the back-angle pion cross sections are large and the data-taking rate was quite good even with the thin targets.

3. Pion detection

The pion detection system (Fig. 1) consisted of three components: (1) A thin front scintillator 30 cm from the center of the target, followed by (2) a set of three multiwire proportional chambers, and (3) the eight-crystal intrinsic germanium telescope in which the pions were detected and their energies measured.

The thin (1.6 mm) front scintillator was used to reduce the trigger rate due to scattered decay muons. This rate was especially high at forward angles for heavy targets.

The main functions of the wire chambers were (1) to confirm that the particle in an accepted event came from the beam spot, (2) to help with the elimination of pulse pileup in the Ge detectors, and primarily (3) to limit the accepted events to particles passing through the Ge telescope within a specified distance from the telescope axis. This limits the effects of pion outscattering in the detector. During the initial runs the wire chambers used delay line readout. In later runs they were replaced by a set of chambers with individual readouts from each of the wires.

The particle identification and pion energy determination were carried out on the basis of signals in the intrinsic germanium telescope. This detector was built by the Lawrence Berkeley Laboratory semiconductor detector group in consultation with the medium energy physics group at Carnegie-Mellon[15] University. It consists of eight 4 cm diam germanium crystals. The crystals are held in place in a copper holder which is in contact with liquid nitrogen in a Dewar. Annular rings made of boron nitride provide the crystals's thermal contact with the copper holder. These so-called "cold fingers" have a 3.5 cm diam hole through which the detected particles pass.

The first two crystals are 0.25 and 0.5 cm thick. The remaining six crystals are about 1.2 cm thick. The total detector thickness is 43 g/cm^2 of germanium which is enough to stop 100 MeV pions.

Since this is the first study of inclusive pion spectra using an intrinsic Ge telescope, the relevant properties of the detection system have been described in detail. The choice of germanium for the telescope material was based in part on its better energy resolution than that of plastic scintillators. Better resolution makes it easier to distinguish pions from muons, a feature which was especially important at the more forward angles.

One advantage of a multicrystal germanium telescope over a magnetic spectrometer is that it allows one to measure a full pion spectrum at the same time. Another advantage is that, because of the shorter flight path, fewer pions decay in flight between the target and the detector. This is most important at the low energy end of the spectrum. The main disadvantage of any telescope is that one cannot use it to detect negative pions since these leave "stars" of varying pulse height when they come to rest at the end of their range.

B. The electronics and data acquisition

The primary data for each detected particle consisted of the pulse heights (particle energy losses) in the Ge-telescope crystals and the position coordinates of the particle trajectory in each of the three wire chambers. The full set of data for each event which passed the requirements set by an acceptance trigger was stored on magnetic tape for later analysis.

1. Pion acceptance trigger

There were four components in the acceptance trigger, all of them designed to limit the recording of background events without affecting the system's efficiency for scattered pions. Since the data collection rate in many of the runs was limited by the rate at which events could be recorded by the computer, and since many charged particles other than scattered pions passed through the detectors, the design of the acceptance trigger was a critical part of the experiment.

(1) The particle was required to pass through the first germanium crystal and to deposit a minimum amount of energy in the second one. (The requirement of Ge2, a fast pulse from the second crystal, in addition to Ge1, a fast pulse from the first, did not reduce the rate of recording useful pion events since information from at least two crystals was needed for eventual particle identification.)

(2) A signal, FS, was required from the front scintillator to make sure that the detected particle came from the beam spot on the target.

(3) To reject protons a threshold was set on the output of each germanium crystal using fast discriminators. These thresholds were set to be safely higher than the maximum pulse height which a pion could produce in the crystal. The signals for these oversized pulses were combined in a logical "or" whose output, p, was used to veto the trigger. This veto rejected the bulk of the protons since in most cases a proton's energy loss exceeded the threshold in at least one crystal.

(4) The elimination of signals from electrons was also handled using fast signals from the germanium crystals but the rejection system was somewhat more complicated than it was for protons. First, the crystal in which the particle stopped was determined using the coincidence between fast signals from the crystals. For example, the particles stopping in crystal 3 were identified by the signature $\text{Ge1}\cdot\text{Ge2}\cdot\text{Ge3}\cdot\overline{\text{Ge4}}$. Particles depositing less energy than a prescribed threshold in the crystal immediately before the stopping crystal (Ge2 in this case) generated a signal, e. This threshold in Ge2 (or equivalent) was set safely below the smallest possible energy loss for a pion that passed through the crystal. The use of e as a veto acted to suppress electron events. In summary, the trigger consisted of

$$\text{FS}\cdot\text{Ge1}\cdot\text{Ge2}\cdot\bar{\text{e}}\cdot\bar{\text{p}}\ .$$

Incidentally, it was possible to reverse the $\bar{\text{e}}$ or $\bar{\text{p}}$ logical requirements so that we could accept only those particles which were normally rejected. Thus it was possible to analyze the normally rejected particles with the full computer based particle identification to ensure that no pions were being rejected.

The range-energy relations for muons are not sufficiently different from those of pions for muon rejection to have been included in the trigger. Muon elimination had to be carried out for the stored events using the particle identification scheme described below.

2. Counting rates and dead times

At forward angles, the high singles rates in both the germanium detector and wire chambers made it necessary to reduce the intensity of the incident beam. Placing lead bricks upstream from the counters also helped considerably in keeping the singles rates at acceptable levels. It was found however that at angles forward of 40°, the high muon background rate made the collection of useful data impossible. These muons were produced in pion decays upstream from the target, and were elastically scattered in the target and surroundings.

A significant dead time for the data collection arose from the triggers which occurred during the time that the computer was busy reading an event. To correct for these, a busy signal was generated by each accepted trigger and was reset when the computer had completed storing the event. Events whose triggers occurred during this time were not collected and their triggers were counted. The ratio of the total number of triggers to the accepted triggers provided the correction factor for the computer dead time. The correction factor for most of the runs was less than 1.5.

An additional dead time came from the stretcher-multiplexer which processed the linear signals. It took about 1 μs to reset the stretcher and any pulses appearing during this μs were rejected. Their triggers were counted and used to compute a "stretcher-reset" dead time.

3. Detector calibrations

The pulse heights of the germanium crystals were calibrated in terms of energy by using gamma ray sources in conjunction with a precision pulser. The calibration was checked during the experiment with a CH_2 target. The measured position of the πp scattering peak was found to agree within $\frac{1}{2}$ MeV with that expected from the γ-ray calibration. Runs with the detector directly in the pion beam provided a further check on the energy calibration. These checks were reassuring since typical energy depositions by pions in the crystals are an order of magnitude larger than those from the gamma rays.

The wire chamber coordinate system was lined up with the target and detectors by using a special target made of wires. The horizontal position resolution in both types of wire chambers was $\simeq$1 mm. In the vertical direction, the resolutions were 2 mm for the delay line chambers and 1 mm for the individual-wire read-out chambers. These values correspond to a resolution of 5 to 8 mm in the horizontal direction at the target (where the beam spot size was typically 5 cm wide and 3 cm high). They also correspond to $\simeq$1.5 mm uncertainty at the front of the Ge telescope.

4. Linear signals

The signals from the individual Ge crystals were amplified and their pulse heights measured with analog-to-digital converters. There was one special problem in the determination of pion energies which arose from the short (2.2 μs) decay time of the pion's decay muons. The posi-

tive electrons from the muon decay have energies up to 52 MeV, some of which would generally be deposited in the germanium crystals. To identify and eliminate events which included electron pileup, the linear Ge signals were processed by two independent amplifiers with different integration times (200 and 800 ns). The 800 ns system was used to assign pulse heights because of its better resolution. By comparing signals from the two systems it was possible to correct for events where the muon decayed between 200 and 800 ns after the pion stopped.

C. Data analysis

The raw data were analyzed to obtain cross sections in mb/sr MeV as a function of outgoing pion energy. There are four main components in this analysis.

1. Particle identification (PID)

Particle identification was accomplished by comparing the total measured energy, E, from all crystals with the sum, E', for all but the stopping crystal. (In cases where the pulse height in this crystal corresponded to less than 5 MeV of energy, the "stopping crystal" was defined to consist of the last two crystals in which energy was deposited.) The nominal mass of a stopped particle was determined from these two energies by reference to a table based on an empirical range-energy relation. The closeness of stopping powers for pions and muons was not so troublesome as one might at first expect. The 4 MeV muon pulse from the decay of the stopped pion acted to increase the apparent mass of the pions, and thus helped to distinguish them from muons.

The contamination of the pion data by muons, electrons, and protons is estimated to be less than 10% at all angles back of 50°. At 40°, the muon contamination of the raw pion spectra could be as much as 30%. We believe that we have been able to remove most of this contamination by examining the scatterplot of energy versus the PID value for each accepted event. The uncertainty in this removal is estimated to be about $\frac{1}{3}$ of the subtracted amount. To achieve these levels of certainty, the pulse height in *each* crystal was compared with the expected pulse height based on the measured particle energy (total pulse height) and pion range-energy tables. The root mean square deviation between measured and expected pulse heights was required to be within specified limits. The need for this detailed look at the individual pulse heights arose from the presence of events where protons or muons managed to pass the original pion-identification criterion as a result of outscatterings, nuclear reactions, pileups, etc.

2. Energy determination

The pion energies were determined on the basis of the calibration described in Sec. II B 3. There were two special problems associated with the detector characteristics.

The presence of dead layers on the faces of the crystals led to small inaccuracies in some energy determinations, especially for those particles stopping in or just beyond a dead layer. For the particles passing through a dead layer, a correction was applied for the undetected energy lost in the dead layer. Such a correction could not be made for particles which stopped in a dead layer. The effect of particles stopping in a dead layer was to deplete the apparent yield in a narrow region of the energy spectrum with a corresponding enhancement in a region just below it.

Another detector feature that affects the energy measurement is the degradation of pions which pass through any of the annulus-shaped cold fingers between the crystals. To minimize such effects the pion trajectories were required to pass through the front face of the first crystal within 1 or 1.2 cm from the detector axis. (The inner radius of cold finger is 1.75 cm.) This restriction also reduced possible errors due to the outscattering of the particles toward the end of their range.

3. Efficiency determinations and flux normalization

The absolute cross sections, per unit solid angle per MeV, $(d^2\sigma/d\Omega\, dE)_x$ for a target, x, were determined from the measured number of counts using the standard relation

$$(\text{counts/MeV})_x = (d^2\sigma/d\Omega\, dE)_x\, n_x\, (\text{pion flux})_x \epsilon(E_\pi)\ ,$$

where n_x is the number of target nuclei per cm^2 and $\epsilon(E_\pi)$ is the overall system efficiency (effective solid angle times the intrinsic efficiency). Since we were measuring the pion spectrum over a wide energy range, it was necessary to have the correct pion detection efficiency as a function of energy. The product of the last two factors was obtained by measuring the elastic scattering of pions from hydrogen in a polyethylene target using the corresponding relation:

$$(\text{counts})_{\text{H}} = (d\sigma/d\Omega)_{\text{H}}\, n_{\text{H}}\, (\text{pion flux})_{\text{H}} \epsilon(E_\pi)\ .$$

For $(d\sigma/d\Omega)_{\text{H}}$ we used the results of a phase shift analysis of the measured elastic πp cross sections.[16] The background from the carbon in the CH_2 was subtracted by using the spectra from a pure carbon target.

The pion fluxes were monitored by the downstream ion chambers. Except for a few runs with the thickest high Z targets, the counting rate in the ion chambers was found to be independent of the target and its thickness, as confirmed by normalization to the counting rate of the primary-beam protons of the LAMPF accelerator.

With a given incident pion energy, it was possible to determine the value of the product, (pion flux) $\epsilon(E_\pi)$, at only a discrete number of values of outgoing pion energies E_π, each value corresponding to some chosen scattering angle. It was therefore necessary to interpolate to obtain a continuous efficiency curve. The efficiencies so determined were only relative since at no time was the absolute pion flux measured. The absolute calibration was achieved through the normalization to scattering from hydrogen.

The shape of the measured efficiency curve compared very well to one determined by a Monte Carlo calculation. [The calculation shown (Fig. 2) corresponds to a maximum off-axis acceptance radius of 1.0 cm at the entrance of the Ge telescope.] The efficiency curve falls off gently

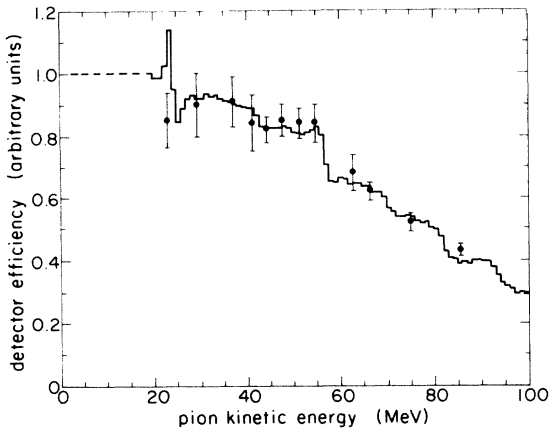

FIG. 2. The efficiency of the germanium telescope as a function of pion energy. The curve is the result of a Monte Carlo calculation. The data are from measurements of the known (Ref. 14) π-p cross section.

at first due mainly to nuclear interactions and eventually (at $\simeq$60 MeV) it falls more rapidly as pions begin to escape from the sides of the Ge telescope as a result of multiple scattering.

The system efficiency $\epsilon(E_\pi)$, as it has been defined, includes wire chamber efficiencies. Some of the otherwise acceptable pion events were not accompanied by an unambiguous set of wire chamber readings. The fraction of events that had to be rejected because it was not possible to construct the necessary pion trajectory depended on the counting rate and the pion energy. It was possible to determine wire chamber efficiencies as a function of pion energy for each run from the data of that run. These efficiencies were typically higher than 70% with the delay-line chambers and higher than 85% for the individual-wire readout chambers.

4. *Subtraction of the elastic peak*

In order to be able to correct the inelastic spectra for the tail on the elastic peak (especially important at forward angles), we measured the pion energy spectrum with the detector placed directly in the beam. The observed peak shape was used to subtract the effects of the elastic line after it was appropriately broadened to take into account straggling in the target and the momentum width of the pion beam. This procedure was checked by fitting the 100° carbon spectra where the excited states are well resolved. The uncertainty in the counts attributed to the elastic tail is typically about 15%. At 40 deg, the elastic tail which is subtracted constitutes 10—20% of the observed inelastic spectrum. It falls to less than 5% of the spectrum by 60 deg and becomes much smaller at larger angles.

III. EXPERIMENTAL RESULTS

A. Spectra of scattered pions

The results of this experiment are a set of over 100 spectra for scattered positive pions. Figure 3 shows a sample of these spectra for our lightest target, carbon, at

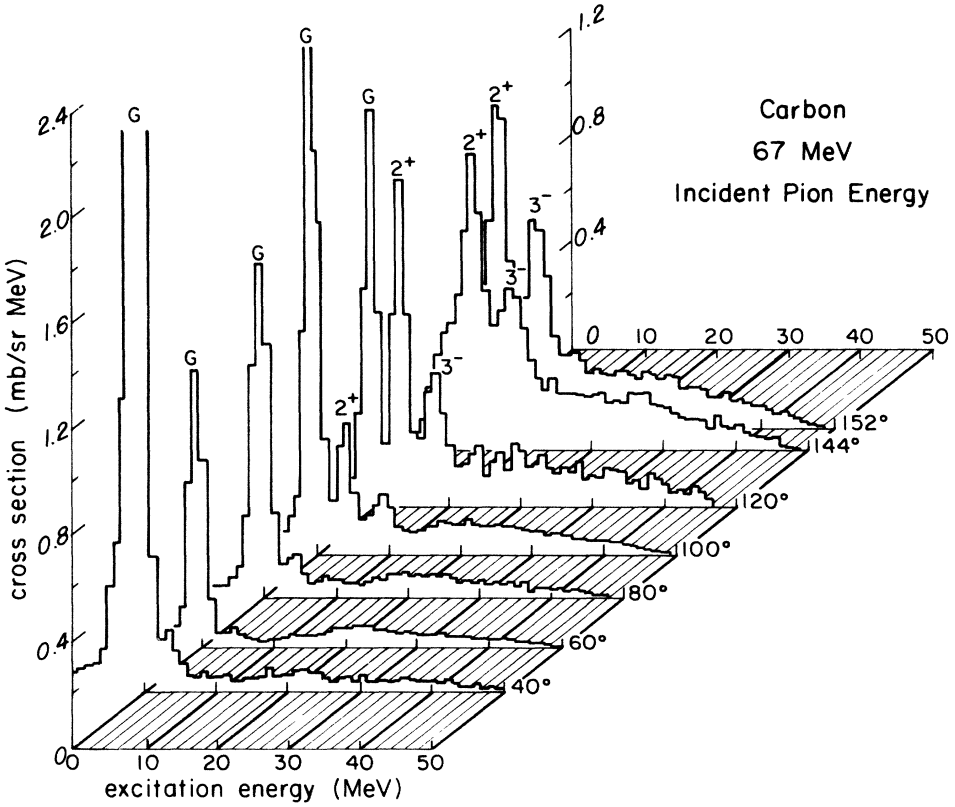

FIG. 3. Differential cross sections per unit pion energy for the scattering of positive pions from carbon at angles from 40° to 152° at our lowest incident energy. Statistical uncertainties in this and subsequent figures can be judged (except in regions where individual states are strongly excited) by the fluctuations of the spectrum about a smooth curve through the data.

an incident energy of 67 MeV. The ordinate is the double differential cross section $d^2\sigma/d\Omega\,dE$ in units of mb/sr MeV. The abscissa is the excitation energy of the residual nucleus. For clarity, error bars have been omitted in the spectrum figures in this paper. Except in the region of strongly excited individual states, the local statistical uncertainties can be judged from the fluctuations of the spectra about a smooth curve.

It is seen that the carbon 2^+(4.4 MeV) and 3^-(9.6 MeV) inelastic states are strongly excited only at backward angles just as one would expect on the basis of the small amount of orbital angular momentum which is brought into a carbon nucleus by 67 MeV pions ($l \leq 2$). Although it was not our main purpose to study the cross sections to individual states, these carbon measurements, together with the elastic cross section measurements on all targets, provide a useful check on the accuracy of our measurements by permitting comparisons with earlier results. Our cross sections for carbon at 67 MeV are in excellent agreement with those of Amann *et al.*[17] (which were, however, measured with the same detector). Our results at 85 MeV are also in quite good agreement with those of Blecher *et al.*[18] obtained at 80 MeV with a magnetic spectrometer.

Figure 4 shows the carbon spectra at our highest incident energy, 100 MeV. The cross sections to individual low-lying states are lower at 100 MeV than those at 67 MeV, but the average cross section per MeV at higher excitations is somewhat larger. The continuum portions of these spectra are similar in *shape* to those of Ingram *et al.*[19] on oxygen at 114 MeV. They also agree well in *magnitude* when they are adjusted for the differences in target mass and incident energy using the empirical dependences determined from the present measurements.

Spectra for our heaviest target, lead, corresponding to the two for carbon, are given in Figs. 5 and 6. To show the changes which occur in the spectra as a function of target mass, the spectra for our four main targets taken at an intermediate incident energy (85 MeV) are plotted in Fig. 7 for a forward angle and a backward angle (60° and 152°). It is seen here and in the earlier figures that the elastic cross sections drop off as one goes to backward angles whereas the inelastic continuum cross sections increase considerably.

Finally in Fig. 8, we show spectra for an intermediate mass target, calcium, at 80° for the three main bombarding energies used in our measurements.

The spectra for the heavier targets appear to be rather smooth and structureless at higher incident energies and higher excitation energies. The tin spectra do, however, show a conspicuous peak at an excitation of 6.5 MeV (Fig. 9) and in Ca there is a definite broad bump in the 67 MeV spectra at excitations near 18 MeV (Fig. 8). To make sure that the latter bump was not simply due to some instrumental artifact, the spectra were remeasured with a sequence of absorbers of different thickness between target and detector. The bump was found to shift and to broaden with increasing target thickness by appropriate amounts.

B. Angular distributions of the inelastically scattered pions

The energy-integrated spectra at the different incident energies are plotted in Fig. 10 as a function of $\cos\theta$ where θ is the scattering angle in the laboratory frame. In making these plots, the elastic peaks (and their tails) were subtracted from the observed spectra. As has already been

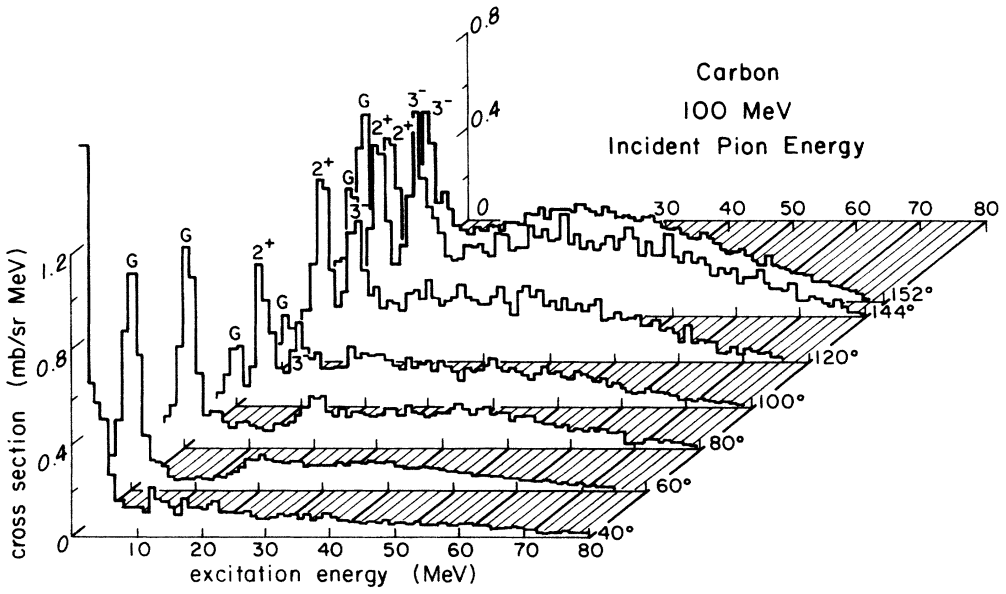

FIG. 4. Differential cross sections per unit energy for the scattering of positive pions at angles from 40° to 152° at our highest incident energy.

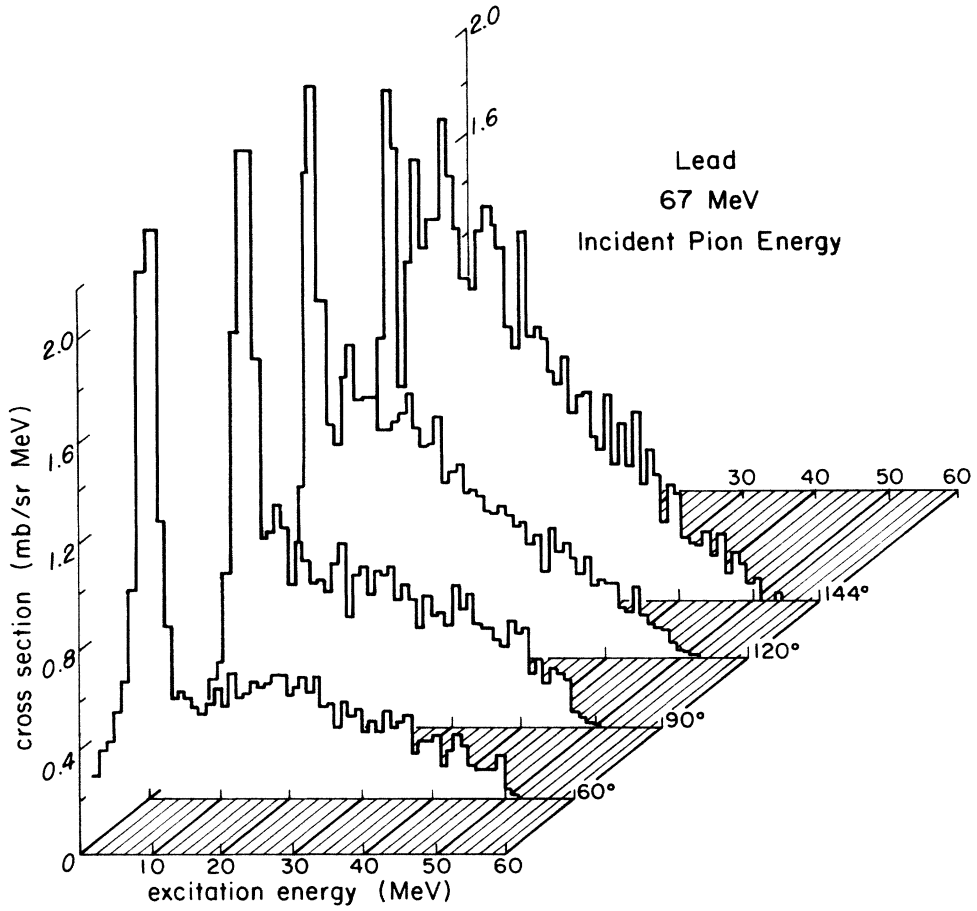

FIG. 5. The cross sections for lead corresponding to those for carbon in Fig. 3.

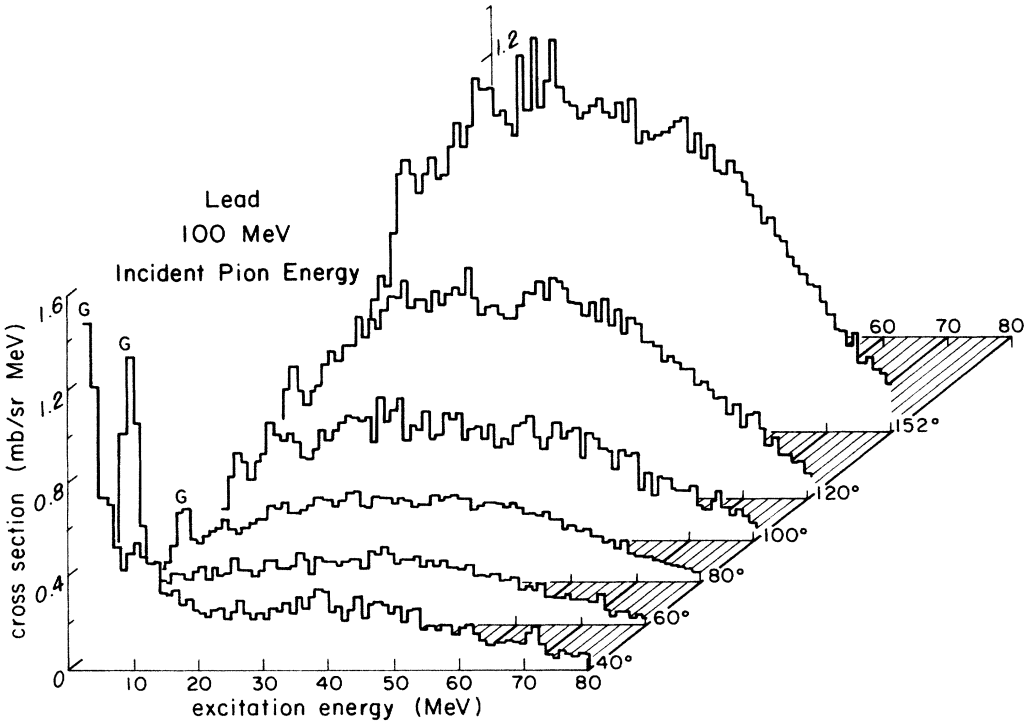

FIG. 6. The cross sections for lead corresponding to those for carbon in Fig. 4.

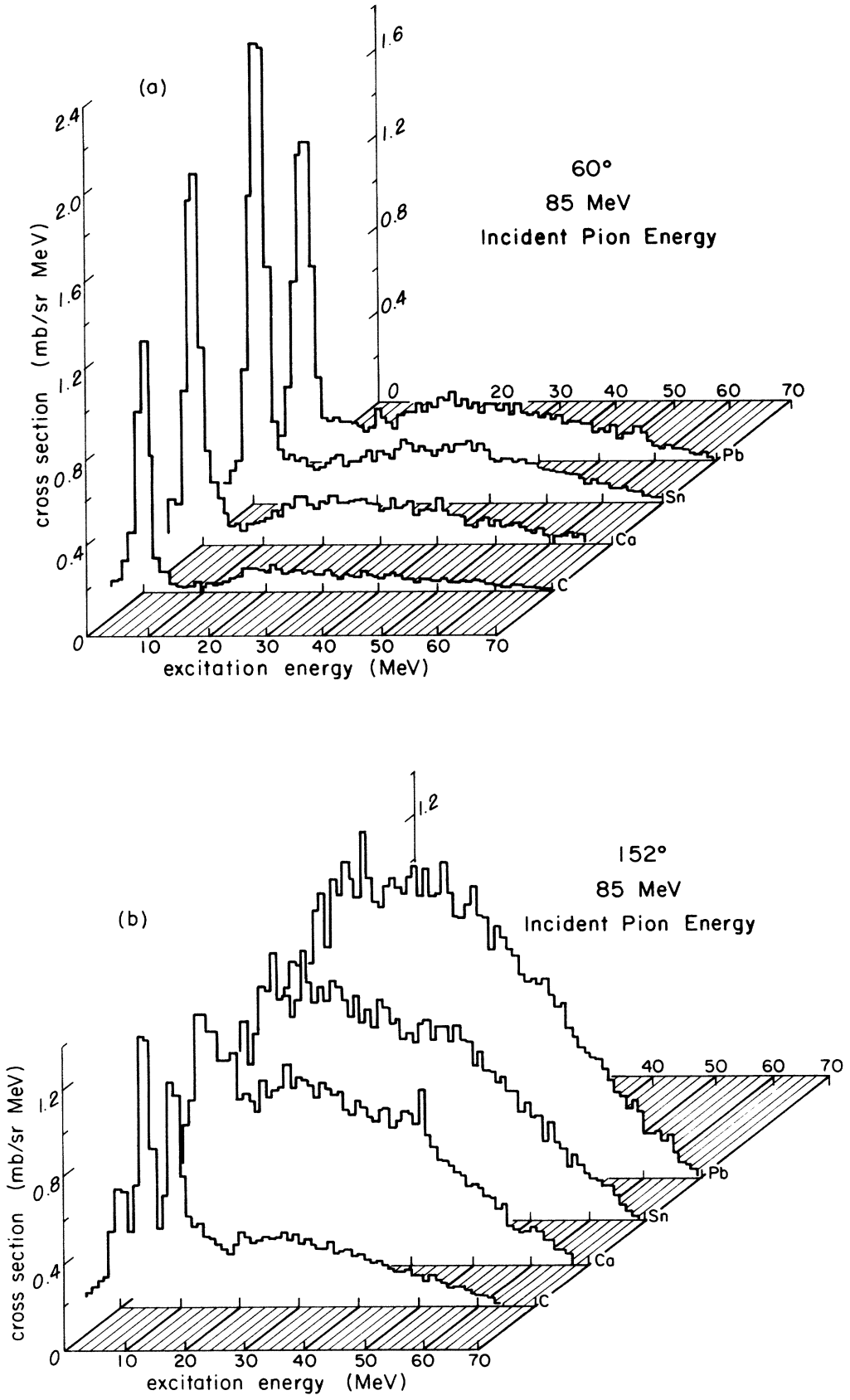

FIG. 7. The differential cross sections per unit energy for the scattering of positive pions for the four main targets at 85 MeV and (a) a typical forward angle and (b) a typical backward angle.

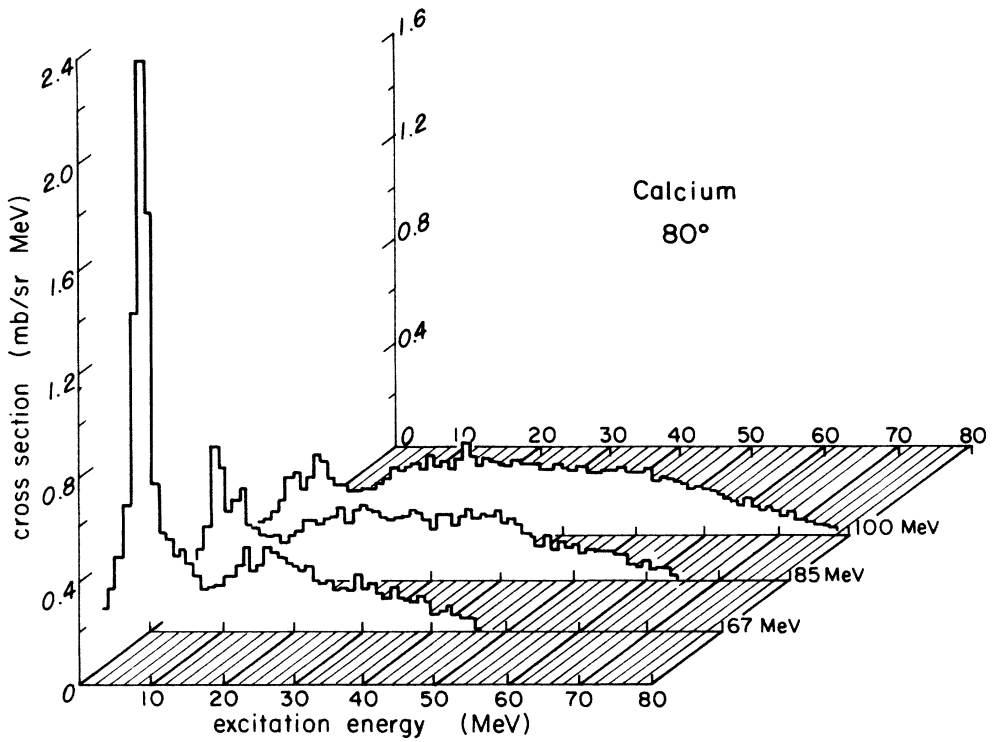

FIG. 8. The differential cross sections per unit energy for the scattering of positive pions from calcium at 80° for three incident energies.

mentioned, this subtraction introduces uncertainties of less than a few percent except at the most forward angles where the uncertainties can be as large as 15—20%. The spectra must also be corrected at their high-excitation-energy end because of the low-energy cutoff in the detector. This cutoff is fairly sharp at ~18 MeV. Fortunately, the cross sections are small and falling rapidly where the cutoff occurs. The uncertainties in the total inelastic cross sections due to the extrapolation of the spectra to excitation energies above the cutoff are estimated to be no greater than 5%.

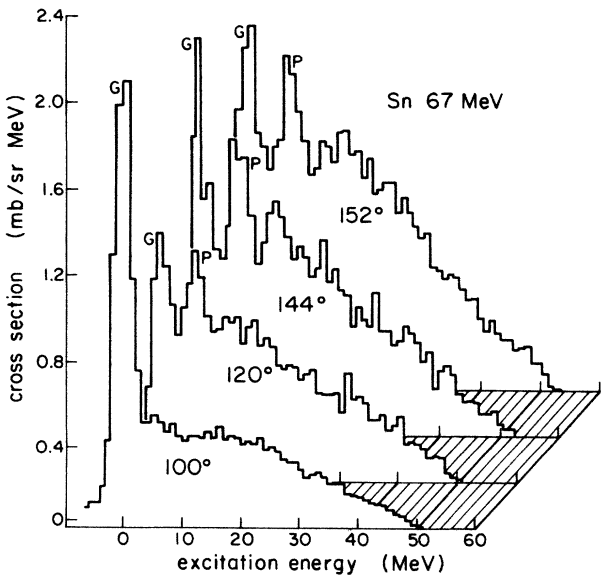

FIG. 9. The differential cross sections per unit energy for the scattering of positive pions from Sn at 67 MeV for a number of angles. A strong inelastic peak P centered near ~6 MeV is seen to appear at the backward angles.

Two particular reservations relevant to the angular distributions of Fig. 10 must be mentioned. For angles greater than 120° ($\cos\theta < -0.5$) it was necessary to orient the targets in reflection rather than in transmission geometry. Runs using both geometries were made at 90° and 120° to check the consistency of the two types of measurements. There was a 15—18% discrepancy at 120° and an 8% discrepancy at 90° between measurements using the two target geometries. This still unexplained discrepancy is in striking contrast to other tests of run repeatability. Repeats of measurements for a given target at a particular angle generally agreed to within ±2% even when the runs being compared were done in different run cycles and with somewhat different experimental setups. Because of the relatively poor agreements of the 120° tests, the points at 144° and 152° taken in reflection geometry have been assigned added uncertainties of ±8%. They were not normalized to the runs taken in transmission geometry.

A second reservation about the data plotted in Fig. 10 applies at the small-angle end of the angular distributions. The 40° yields for the heaviest targets at 67 MeV were assigned substantial systematic uncertainties. In these runs, the separation between decay muons and pions in two-dimensional plots of the particle-identification signals versus particle energy was not so clean as it was in all other runs.

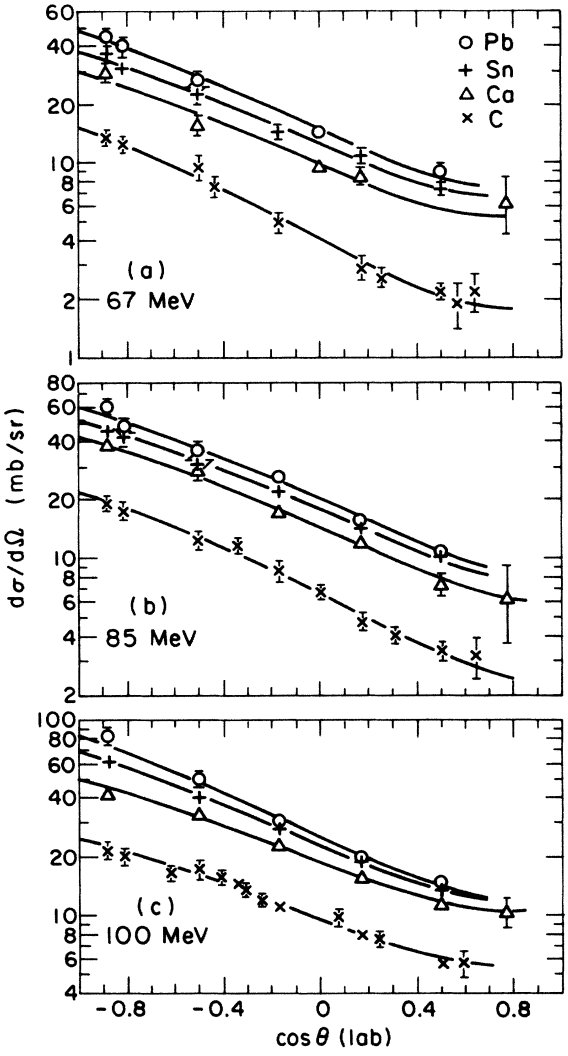

FIG. 10. The angular distributions of the energy-integrated differential cross sections as a function of the cosine of the scattering angle for three incident energies. The curves were determined as described in Sec. III C.

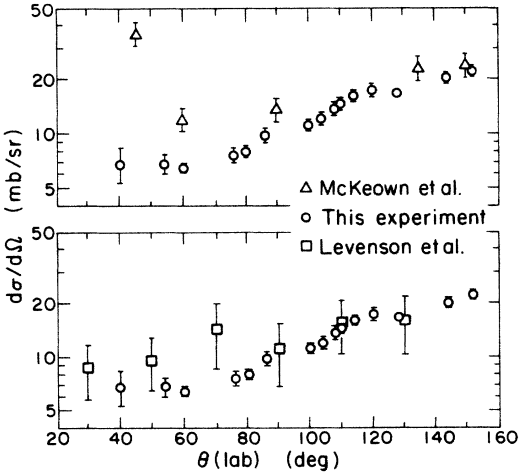

FIG. 11. A comparison of our energy-integrated differential cross sections for carbon at 100 MeV with the earlier work of (a) McKeown *et al.* (Ref. 4) and (b) Levenson *et al.* (Ref. 5).

TABLE I. Measured[a] total $(\pi^+,\pi^{+'})$ inelastic cross sections (mb).

Target	Incident energy (MeV) 67	85	100
C	71±8	108±11	146±13
Ca	159±19	228±25	288±26
Sn	203±25	278±31	364±36
Pb	246±33	319±35	416±38

[a]These cross sections were determined from a smooth surface through the cross-section data plotted as a function of θ and A.

Our results for the angular distributions of positively scattered pions agree within the estimated uncertainties with the results of the Argonne group[4,5] as one can see from Fig. 11. The data of McKeown *et al.*[4] include elastically as well as inelastically scattered pions and it is for this reason that they diverge from ours at forward angles.

C. The dependence of the inclusive scattering cross sections upon target mass number and incident energy

The total inelastic scattering cross section for any target and energy is 2π times the area under the angular distribution curve plotted linearly as a function of $\cos\theta$. In extracting these total cross sections (Table I) it was assumed that the spectra change smoothly with mass number A as well as with angle θ. This assumption acts to minimize variations in the *shapes* of least square polynomial fits to the angular distributions as one goes from target to target.

The smoothing was carried out by taking as a reference distribution, the least-squares fit to the average angular distribution for all targets. The distribution for a particular target $d\sigma/d\Omega$ (θ,A) was then written as $N_A[1+\alpha(A)\cos\theta+\beta(A)\cos^2\theta]$ times the reference distribution. The three constants here were determined by least squares fits to the data. The coefficient $\alpha(A)$ measures the change in the mean tilt of the distribution for target A from that of the average distribution of Fig. 10. The coefficient $\beta(A)$ measures a mean curvature difference and N_A provides the normalization. The fact that there are only two shape-related constants in the correction function limits the *variations* in shape between the best-fit solutions for different A. The fact that the β's in the fits so determined were often too small to be distinguished from zero shows that the measured data are not at all inconsistent with the assumption of only minor changes in the distribution shape from target to target.

The angular distribution curves plotted in Fig. 10 were determined in this way. From these curves, one can easily read off the extrapolated cross sections at 180°, $d\sigma/d\Omega$ (180°). These were found to be particularly useful (see Sec. VI) for the interpretation of results and are plotted in Fig. 12 as a function of A.

IV. A CLASSICAL MODEL FOR THE INTERPRETATION OF THE DATA

A. Evidence for the dominance of quasielastic scattering in the inclusive spectra

It is generally accepted that the observed inelastically scattered pions, in the energy range near the (3,3) reso-

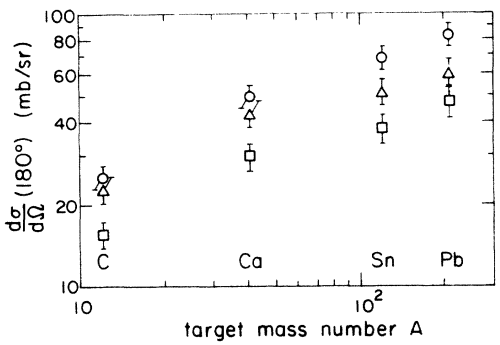

FIG. 12. The measured differential $(\pi^+,\pi^{+'})$ cross sections (extrapolated to 180°) as a function of target mass number A at 67 MeV (□), 85 MeV (△), and 100 MeV (○). The uncertainties shown include systematic as well as statistical components. Relative uncertainties between different targets at any one incident energy are about half as large as those in the figure.

nance, are mainly quasielastic pions. That is, they are the products of a strong encounter of the incident pion with just one of the nucleons in the nucleus. We briefly review the major evidence for this picture.

1. The angular distribution of pions scattered from nuclei

These distributions peak sharply backward just like those in pion scattering from free nucleons. In fact they are somewhat more anisotropic than the latter. For example, the 180°/90° cross-section ratio at 100 MeV is 1.9 in the laboratory frame for $\pi^+ + p$ whereas it is 3.2 for pions on lead (Fig. 10). One can think of a number of reasons that this ratio would be larger for sizable nuclei than it is for hydrogen.

(a) Most pion-nucleon interactions in the nucleus occur on the upstream side of the nucleus (as we argue below). The average escape path length from such sites is smallest for emissions back along the incident trajectory and the escape probability is therefore greatest at 180°.

(b) The energy loss of the pion is, on the average, larger the more backward the scattering. Lower pion energy favors a pion's escape since the pion-nucleon cross sections fall rapidly with decreasing energy below the (3,3) resonance.

(c) Because the nucleons in the nucleus are moving there is an additional consequence of the strong dependence of the π-nucleon cross section on energy. The chance for head-on pion-nucleon collisions is greater than that for catch up collisions. Since the laboratory angular distribution of the former is more backward, this too acts to increase the backwardness of the π' angular distributions from nucleons when they are inside nuclei.

These various effects all act to increase the backward anisotropy from single collisions of pions with nuclear nucleons. Their effect on the anisotropy of the inclusive scattering cross section apparently overcomes those due to the spread in scattering directions due to the Fermi motion of the struck nucleons, to multiple scattering and to the contributions from π^+-n scattering, all of which would act to make the angular distribution more isotropic.

2. The shapes of the spectra of inelastically scattered pions

The central energies and widths of the observed spectra are roughly consistent with the assumption that the pions are scattering from nucleons which have momentum distributions typical of nuclear matter. This is seen more clearly in spectra at higher incident energies where the quasielastic peaks are not so broad as those of the present measurement.

3. The size of the $(\pi,\pi+$nucleon$)$ reaction cross sections

The cross sections for a pion to eject a single nucleon from a nucleus, with no further particle emissions, can often be determined from the induced radioactivity. These cross-sections tend to be rather large, reaching values over 20% of the total reaction cross section[20] (and a much larger fraction of the inclusive scattering cross section).

4. The observation of coincidences between scattered pions and ejected nucleons

Measurements of coincidences between inelastic pions and nucleons which are simultaneously emitted from a nucleus show that a large fraction of the inelastic pions have undergone nearly free collisions with single nucleons.[21]

B. Elements of the classical model for the scattering of pions from nuclei

In this paper we will restrict our attention mainly to two kinds of cross sections, the total reaction cross sections and the backward-scattered $(\pi^+,\pi^{+'})$ differential cross sections. Assuming, on the basis of the foregoing independent evidences that the backward differential cross section is largely due to quasielastic (single scattering) events, this cross section and the reaction cross section depend on only the very first collision of the pion entering the nucleus. (All events with at least one collision contribute to the reaction cross section.) The analysis of these two cross sections must therefore be considerably simpler and therefore more critical to the basic assumptions of any model invoked in their explanation than cross sections which depend on later, more uncertain, stages of the nuclear cascade.

We will deal with the backward differential cross section in terms of the cross section at 180°. There are two reasons to focus one's attention at 180°. (1) As we will show in the next section, the model calculations of the quasielastic component are simplest and most transparent when the pions enter and exit the nucleus along the same path. (2) The differential cross section is almost certainly least contaminated by contributions from multiple scattering in the nucleus for those scatterings which are observed at 180°. This is because the quasielastic cross section is largest at 180° whereas the multiple-scattering yield is most probably rather isotropic. The most direct evidence in support of the latter statement is the observed near-isotropy[22] of inclusive double charge exchange scattering of pions from nuclei. Since the free π-nucleon angular distribution for single charge exchange is quite similar to that without charge exchange, it is reasonable to assume that the $(\pi^+,\pi^{+'})$ distribution is isotropic like that for double charge exchange when it is due to two or more

scatterings in the nucleus. This rapid homogenation in direction in pion multiple scattering compared, for example, to the much slower one for protons (familiar from cascade calculations) stems from the fact that, for π plus nucleon, the angular distribution from the basic two-particle encounter happens to be backward rather than forward peaked.

Assuming isotropy for the multiple-scattering component, it follows from the observation that the ratios of the maximum to the minimum differential cross section (Fig. 10) are all about 5:1 that at least 80% of the 180° scattering cross section can be attributed to single-collision scattering. For simplicity we will assume that the *entire* measured cross section at 180° is quasielastic. In what follows we will see how well a classical picture based on this assumption accounts for the observed dependence of $d\sigma/d\Omega$ at 180° upon target mass number, incident energy, etc.

The quasielastic character of backward pion scattering has often been emphasized by Ashery *et al.*,[6] Ingram,[9] and others. By normalizing the angular distributions which they observed from nuclei to the very similar one for π^+ scattering from free nucleons, they were able to characterize the backward scattering yield by a number, N_{eff}, which represents the "effective" number of nucleons which participate in the scattering. In a heavy nucleus, N_{eff} is found to be less than 10% of the total number of nucleons.

In the present work we have chosen to identify the quasielastic cross section with the extrapolated 180° cross section rather than with the *average* back-hemisphere cross section as in the earlier papers. Our choice is due in large part to the already mentioned difference that we find between the observed shapes of the backward π-nucleus and π-nucleon angular distributions. (The existence of such a difference is no surprise in view of the expected absorption and rescattering effects.)

The interaction parameters used in the model will be chosen to correspond to free particle parameters for the incident pion energy. The results so obtained will require modifications for the pion refraction in the Coulomb and nuclear fields, for changes in the pion's kinetic energy in the nucleus, and for the Fermi motion of the struck nucleons. All of these effects will be looked at individually. We will not try to consider them all at once in a single attempt to predict the measured cross sections since some of them are considerably less certain than others. Instead we will do a number of exercises to help us assess individual magnitudes for each of the several effects which are considered. These exercises will be simple enough to make clear the basic nature of each effect.

Although possible effects of the pion's wavelength, $\lambda\!\!\!^{-}$, will be discussed below, the calculation is unambiguously classical. In describing collisions which lead to distinct residual states in a target it would not make sense to ignore quantum effects, but where inclusive scattering data or integral cross sections are being considered, a classical description can be expected to be reasonably valid.

We start by deriving expressions for the total reaction cross section and the 180° differential scattering cross section based on a picture which involves straight line trajectories for the pions as they go into and out of the nucleus. (The Coulomb and nuclear distortions of the projectile paths are generally small and will be considered separately.)

The incoming pion is assumed to proceed into the nucleus until it interacts with some individual nucleon with which it forms a pion-nucleon complex. If this complex should decay back to a pion plus a nucleon before it collides with another nucleon, the angular distribution of the decay is assumed to be identical with that for the interaction of a pion with a free nucleon. We will call an event of this kind a quasielastic scattering of the pion. Events in which the complex collides with a nucleon before it has had a chance to decay will lead ultimately to pion absorption or to the multiple-scattering component of the inclusive pion scattering cross section.

1. *The form of the total reaction cross section according to model*

In this picture, *all* possible interactions of the pion in the nucleus begin with the formation of a pion-nucleon complex. It is therefore possible to express the total reaction cross section as

$$\sigma_{\text{reaction}}=\int\int 2\pi b\,db\,f(z,b)\,\sigma\,\rho(z,b)dz\ , \tag{1}$$

where σ is the formation cross section of the complex (i.e., it is the the free pion-nucleon scattering cross section) per nucleon. The variable z is the linear coordinate along the pion trajectory at impact parameter b and $\rho(z,b)$ is the nucleon density at coordinate (z,b) in the nucleus. The probability that the pion arrives at (z,b), without having had any earlier collisions with nucleons, is given by the factor $f(z,b)$. This factor, f, measures the attenuation of pion flux and can be written

$$f(z,b)=\exp\left[-\sigma\int^{z}\rho\,dx\right]\equiv\exp[-I_b(z)]\ . \tag{2}$$

The quantity $I_b(z)\equiv\sigma\int^{z}\rho\,dx$ is seen to be the number of collision mean free paths along the trajectory up to the point z. Notice that in terms of I_b the reaction cross section Eq. (1) becomes simply

$$\sigma_{\text{reaction}}=\int 2\pi b\,db\int e^{-I_b(z)}dI_b(z)\ , \tag{3}$$

where the limits on $I_b(z)$ are zero and $I_b(\infty)$. The latter quantity is the value of I_b for the full track length through the nucleus at impact parameter b. Thus

$$\sigma_{\text{reaction}}=\int 2\pi b\,db(1-e^{-I_b(\infty)})\ . \tag{4}$$

We shall have occasion to use this expression for the reaction cross section later. Because the nuclear thickness in larger nuclei tends to be at least a few mean free paths long for values of the impact parameter b which are smaller than the nuclear radius, R, it follows that the magnitude of the pion reaction cross section must be close to that of the geometrical cross section, πR^2. In short, the nucleus is rather black to pions.

2. *Form of the 180° differential scattering cross section according to the model*

The foregoing picture of the pion-nucleus interaction also provides a fairly simple expression for the differential

cross section for the quasielastic scattering of the pion *at* 180°. The probability, per unit solid angle, that a pion whose trajectory is at impact parameter b will scatter at *180°* can be written

$$\left.\frac{dP}{d\Omega}\right|_b = \int f(z,b)g(z,b)\frac{d\sigma}{d\Omega}D(z,b)\rho(z,b)dz \ , \tag{5}$$

where $d\sigma/d\Omega$ is the 180° scattering cross section per nucleon. The quantity g is an attenuation factor, which does for the outgoing pion what f [Eq. (2)] does for the incident pion. The factor D is the branching ratio for the decay of the π-nucleon complex formed at (z,b), back into a pion plus a nucleon before it has had a chance to collide with another nucleon.

The attenuation factor g for pion escape at 180° differs from f in that the cross section σ in the exponent must be evaluated at an energy appropriate to the *scattered* pion instead of the incident pion. If we make the very reasonable assumption that the complex coasts only a negligible distance before it decays, the product fg can be written in terms of a common track integral:

$$f(z,b)g(z,b)=\exp\left[-(\sigma_{\text{in}}+\sigma_{\text{out}})\int^z \rho\, dx\right]$$

$$\equiv\exp[-J_b(z)] \tag{6}$$

whence $dP/d\Omega$ becomes

$$\left.\frac{dP}{d\Omega}\right|_b \left[\frac{d\sigma/d\Omega}{\sigma_{\text{in}}+\sigma_{\text{out}}}\right]\int D(z,b)e^{-J_b(z)}dJ_b(z) \ . \tag{7}$$

The quantities in the large parentheses all refer to pion-nucleon cross sections. To obtain the differential cross section for quasielastic scattering from the whole nucleus at 180°, one need only integrate this expression over $2\pi b\, db$.

$$\frac{d\sigma}{d\Omega_{\text{nucleus}}}(180°)=\left[\frac{d\sigma/d\Omega}{\sigma_{\text{in}}+\sigma_{\text{out}}}\right]_{\text{nucleon}}\int 2\pi b\, db\int D(z,b)e^{-J_b(z)}dJ_b(z) \ . \tag{8}$$

This integral will be evaluated in Sec. VI.

For the present let us use Eq. (7) to obtain an approximate numerical value for the branching ratio D from the measured scattering cross section of, say, Pb at 100 MeV. To do this we factor an average, $\bar{D}$, out of the integral in Eq. (7) and recognize that the remaining integrand has a value close to unity for all b values up to the nuclear radius. It falls off rapidly however for larger b. [See the discussion following Eq. (3).] From this it follows that the 180° scattering cross section from the nucleus as a whole is approximately

$$\frac{d\sigma}{d\Omega_{\text{nucleus}}}(180°)\cong\left[\frac{d\sigma/d\Omega}{\sigma_{\text{in}}+\sigma_{\text{out}}}\right]_{\text{nucleon}}\bar{D}\,\pi R^2 \ . \tag{9}$$

If (1), the scattering of pions were isotropic, and (2), σ_{out} could be considered negligible compared to σ_{in} (because the pion loses considerable energy in 180° scattering and the π-nucleon cross section decreases sharply with decreasing energy) and finally, if (3), one could also neglect the contribution of charge exchange scattering to the σ's, then the factor in parentheses would be simply $1/(4\pi)\cong 0.08/\text{sr}$. Actually, for the energy range in this experiment: (1) $d\sigma/d\Omega$ at 180° is about 1.4 times the average $d\sigma/d\Omega$, (2) $\sigma_{\text{out}}\approx\frac{1}{4}\sigma_{\text{in}}$, and (3) the charge exchange cross section is roughly $\frac{1}{3}$ of the whole scattering cross section. Taking these three factors into account we find that our earlier estimate, $1/(4\pi)$, for the value of the parentheses is changed by about 20% to $\approx 0.06/\text{sr}$. The average $\bar{D}$ is therefore equal to the ratio of the nuclear 180° scattering cross section to 0.06/sr times the geometrical cross section. Since the measured scattering cross section for Pb at 100 MeV is 84 mb/sr [Fig. 10(c)] and the Pb geometrical cross section is about 1700 mb, it follows from Eq. (9) that $\bar{D}$ is ≈ 0.8. Despite the crudeness of the estimate, it is clear that in order to account for the observed 180° scattering there must be a substantial probability for the pion-nucleon complex to decay back into the entrance channel. Thus the small value of N_{eff} compared with the actual number of nucleons in a large nucleus which was observed by Ashery and others is *not* primarily due to the suppression of quasielastic events by absorption or other kinds of collisions. It is due mainly to the large value of the π-nucleon scattering cross section itself and to the consequent shadowing of one nucleon by another. If we define

$$N_{\text{eff}}\equiv\frac{\left.\frac{d\sigma}{d\Omega}\right|_{\text{nucleus}}(180°)}{\left.\frac{d\sigma}{d\Omega}\right|_{\text{nucleon}}(180°)} \ , \tag{10}$$

then (since it is impossible for $\bar{D}$ to exceed unity) N_{eff} can be no larger than πR^2 divided by $\sigma_{\text{in}}+\sigma_{\text{out}}$. For Pb at 100 MeV with reasonable estimates for the σ's [see Eq. (12)], this upper bound is ≈ 35, less than 17% of the number of nucleons in the Pb nucleus.

It should be clear from the foregoing text that the observed quasielastic scattering must occur in a relatively thin layer on the upstream side of the nucleus. The effective thickness of this layer can be estimated by rewriting Eq. (9) in terms of λ_{in} and λ_{out} (the mean free paths in and out). If we define $\lambda_{\text{av}}^{-1}\equiv\frac{1}{2}(\lambda_{\text{in}}^{-1}+\lambda_{\text{out}}^{-1})$ (where the λ's are computed at central density, ρ_0) then

$$\frac{d\sigma}{d\Omega_{\text{nucleus}}}(180°)=\frac{d\sigma}{d\Omega_{\text{nucleon}}}(180°)\,\bar{D}\,\rho_0\frac{\lambda_{\text{av}}}{2}\pi R^2 \ . \tag{11}$$

Aside from the factor $\bar{D}$, N_{eff}, as it was defined above, is seen to be equal to the number of nucleons at central density contained in a volume $\pi R^2\lambda_{\text{av}}/2$. For a large nucleus, at $T_\pi=100$ MeV, the effective nuclear thickness, $\lambda_{\text{av}}/2$, turns out to be almost an order of magnitude smaller than the average nuclear thickness, $4R/3$. This is another way to appreciate the strong shadowing of one nucleon by another.

3. *The pion-nucleon cross sections which are used in the model*

To use the foregoing model to estimate actual cross sections one must specify values for the π-nucleon cross sections σ and $d\sigma/d\Omega$ which appear in the equations [e.g., Eq. (7)]. In the approach we have outlined, σ and $d\sigma/d\Omega$ are assigned the actual measured cross sections for pions with free nucleons. It is however necessary to normalize these cross sections per nucleon in the nucleus. This normalization must vary from nucleus to nucleus since the ratio Z/N does and pion cross sections depend strongly on isospin.

We assume for all nuclei that the protons and neutrons are homogeneously distributed. [The shapes of neutron and proton distributions in nuclei are similar and their outer edges are at most ~ 0.2 fm apart.[23] This distance is small compared to the width of the region in which the first π-nucleon interactions occur (see Fig. 13).]

The total pion cross section per nucleon can therefore be written

$$\sigma=\frac{Z}{A}\sigma_{\mathrm{p}}+\frac{N}{A}\sigma_{\mathrm{n}}\,, \tag{12}$$

where Z and N are the numbers of protons and neutrons in the nucleus. The symbol σ_{p} stands for the free π-proton total cross section and σ_{n} stands for the corresponding cross section with free neutrons. The latter includes charge exchange.

The differential cross section per nucleon at 180° can be similarly expressed,

$$\frac{d\sigma}{d\Omega}=\frac{Z}{A}\left.\frac{d\sigma}{d\Omega}\right|_{\mathrm{p}}+\frac{N}{A}\left.\frac{d\sigma}{d\Omega}\right|_{\mathrm{n}}\,. \tag{13}$$

In this case $(d\sigma/d\Omega)_{\mathrm{n}}$ does *not* include charge exchange and the contribution to $(\pi^+,\pi^{+'})$ at 180° by the neutrons is virtually negligible. The $(\pi^+,\pi^{+'})$ cross section on neutrons is small to begin with and besides it has a forward rather than a backward peaked angular distribution. The values of σ_{n}, σ_{p}, $d\sigma/d\Omega\,|_{\mathrm{n}}$, and $d\sigma/d\Omega\,|_{\mathrm{p}}$ which were used in our calculations are recorded in Table II.

TABLE II. π^+-nucleon cross sections used in the calculations of reaction and differential cross sections.[a]

Incident energy (MeV)	$d\sigma/d\Omega\,\|_{\mathrm{n}}$[b] (180°) (mb/sr)	$d\sigma/d\Omega\,\|_{\mathrm{p}}$ (180°) (mb/sr)	σ_{n}[c] (mb)	σ_{p} (mb)
67	0.01	3.1	11.8	22.5
85	0.06	5.0	17.2	39.8
100	0.2	7.2	24.1	61.1

[a]Based on Ref. 16.
[b]Does not include charge exchange.
[c]Does include charge exchange.

V. THE INTERPRETATION OF REACTION CROSS SECTIONS IN TERMS OF THE MODEL

According to the straight-line trajectory model, the total reaction cross section is given by Eq. (4). The two quantities which enter into the path length exponents, $I_b(\infty)$, of this equation are (i) the total cross section per target nucleon [Eq. (12)] and (ii) the nucleon density, ρ. This density was taken to be of the Woods-Saxon form, $\rho=\rho_0\{1+\exp[(r-R)/a]\}^{-1}$, for all nuclei, and the values of the basic parameters, ρ_0, R, and a, were obtained from best fits to high-energy electron scattering data.[24] The cross sections computed in this way are given in Table III as σ_c.

This table also lists "measured" reaction cross sections at 100 MeV. These were obtained by adding the charge exchange plus absorption cross sections measured by Ashery *et al.*[6] to the inclusive inelastic cross sections directly measured by us (Table I). (Ashery also gives figures for the inelastic cross sections but these had to be arrived at by a series of subtractions and have extremely large uncertainties.) To combine our data with those of Ref. 6, it is necessary to interpolate some of the latter with respect to energy and target mass.

Some estimates of pion reaction cross sections have also been made by summing spallation yields. One such measurement for Au at 100 MeV (Kaufmann *et al.*[25]) gives a π^+ reaction cross section of 1740 ± 402 mb where the large uncertainty comes from estimates of unmeasured yields. This measured value is in good agreement with the measured 100 MeV cross sections for Pb given in Table III. It is however seen from the table that the calculated cross sections lie consistently below the measured ones.

A. Possible corrections to the estimated magnitudes of the reaction cross sections

Although the model which underlies Eq. (4) is simple and unambiguous, it possesses these virtues in part by ignoring a number of somewhat uncertain effects. Since some of these could conceivably change the estimated reaction cross sections by measurable amounts, we consider them below, one at a time. In each case, an attempt is made to gauge the possible magnitude of the particular effect.

1. *The effect of pion refraction by the Coulomb field*

The effect on the cross section of the repulsion of the π^+ projectiles in the Coulomb field of the nucleus can be estimated to sufficient accuracy using the standard nonrelativistic factor $(1-V_C/T_\pi)$ where V_C is the height of the Coulomb barrier at the edge of the nucleus and T_π is the pion kinetic energy. The effects of these correction factors have been incorporated into Table III. They range from a 3% correction (C at 100 MeV) to a 26% correction (Pb at 67 MeV). After these corrections for Coulomb deflection are taken into account, the calculated cross sections at $T_\pi=100$ MeV are seen to be uniformly about three quarters as large as those inferred from measurements.

TABLE III. π^+ reaction cross sections (mb).

Target	Energy (MeV)	Measured[a] cross section σ_m	Calculated[b] cross section σ_c	Calculated[c] cross section σ_{cC}	σ_{cC}/σ_m
C	67		149	140	
	100	312	254	247	0.79
Ca	67		406	357	
	100	746	604	564	0.76
Sn	67		923	740	0.77
	100	1423	1231	1089	
Pb	67		1391	1014	
	100	1896	1757	1479	0.78

[a]The sum of charge exchange and absorption cross sections plus the inclusive inelastic scattering cross section (Table I). The uncertainties in these cross sections range from 10% to over 20%. They come mainly from the absorption plus charge exchange measurements (Ref. 6).
[b]From Eq. (4).
[c]The cross section of the preceding column multiplied by the Coulomb correction factor $(1-V_C/T_\pi)$.

2. The effect of the pion-nucleon range of interaction

In the calculation represented by Eq. (4) the interactions are pictured to occur between point pions and an array of nucleons whose centers are distributed in space according to information from electron scattering. Although this calculation involves the pion-nucleon cross section it does *not* explicitly include the range of the pion-nucleon interaction. Suppose, for example, that the nucleon centers happened to be uniformly distributed within a sphere of radius R_0. According to the model, trajectories at impact parameters $b > R_0$ would not contribute to the cross section at all although there should, of course, be some contribution for impact parameters up to $R_0+\mathscr{R}$ where $\mathscr{R}$ is the range of the pion-nucleon interaction. A lower bound for the magnitude of $\mathscr{R}$ can be made by setting the mean pion-nucleon cross section equal to $\pi\mathscr{R}^2$. This would make $\mathscr{R}$ about 1 fm for 100 MeV pions, a distance which is not negligible compared with nuclear radii. Even so, it is easy to demonstrate that the inclusion of an $\mathscr{R}$ of this magnitude would have only a very small effect on the reaction cross section (Appendix A).

3. The effect of the pion wavelength

Our classical estimate of the reaction cross section ignores the blurring of the effective location of the incident pion due to its wave nature. In dealing with fast neutrons, for example, it has long been customary to approximate the reaction cross section as $\pi(R+\lambda\!\!\!^{-})^2$ where R is the target radius and $\lambda\!\!\!^{-}$ is the neutron wavelength. Should such an expression be considered for pions? [Pions with energies between 67 and 100 MeV have $\lambda\!\!\!^{-}$'s comparable to those of the neutrons (with $E_n < 15$ MeV) for which this expression is generally used.] In Appendix B we show that the form $\pi(R+\lambda\!\!\!^{-})^2$ is questionable for *any* projectile. It does not make sense to add $\lambda\!\!\!^{-}$ to the target radius or to the effective radius deduced from Eq. (4). The actual effect of $\lambda\!\!\!^{-}$ is closer to that of the interaction range considered above. It acts roughly as the resolution width of a measuring function and therefore contributes to the effective nuclear radius roughly in quadrature ($R^2 \rightarrow R^2+\lambda\!\!\!^{-2}$) instead of linearly. This leads to a correction of only a few percent.

4. The refractive effect of the pion-nucleus potential

In Appendix C we find that for 100 MeV pions, the reaction cross section increases by about 2.5% for every 10 MeV increase in the real part of the well depth of a Woods-Saxon-shaped pion-nucleus potential. Now the real potential for pions almost certainly is not of the Woods-Saxon shape, but in judging effects of wave distortion (refraction) by a potential, it is nonetheless reasonable to use our Woods-Saxon-based estimate, so long as we choose its depth to reproduce the potential depths in the nuclear surface region which are given by optical potentials fitted to pion elastic scattering. Such potentials are found to be about 20 MeV deep in the surface region.[26] It takes a Woods-Saxon well about 40 MeV deep at the center of the nucleus to reproduce this surface potential. It follows that one can expect about a 10% increase over the calculated cross sections given in Table III when the refractive effect of the nuclear potential is taken into account. This correction is a step toward closing the gap between the magnitudes of observed and calculated reaction cross sections but does not, by itself, account for the whole difference.

5. The effect of the change in pion's kinetic energy arising from the Coulomb and nuclear potentials

In estimating the magnitude of the nuclear reaction cross section on the basis of pion-nucleon cross sections, it is important to pay close attention to the kinetic energy of relative motion between pion and nucleons since the π-nucleon cross sections are strongly energy dependent between 67 and 100 MeV. In the surface of the nucleus, where most of the π-nucleon interactions can be assumed to occur, the incident energy of a positive pion on Pb is reduced by about 15 MeV by the Coulomb repulsion. The corresponding effect of the *nuclear* potential on the effective π-nucleon collision energies is not so clear because of the nonlocality of the pion-nuclear potential. If we assume, nevertheless, that one can use the empirical optical potentials, deduced from elastic scattering, to determine the effective collision energies, one must add about 20 MeV for all targets to the incident energies for both positive and negative pions.[26] Thus, for positive pions the nuclear and Coulomb energy shifts in heavy nuclei are roughly equal and opposite. For light nuclei, the nuclear shift dominates.

To make this discussion somewhat more quantitative, we note that at a pion energy of 100 MeV, a 10 MeV increase in pion energy leads to about a 30% increase in the π-nucleon cross section.[16] The effect on the nuclear *reaction* cross section is, of course, smaller since a good portion of the nuclear cross section is associated with small impact parameters for which the nucleus is already black. The ratio of the fractional change in the nuclear reaction cross section to that for pions on nucleons can be shown to be

$$F=\frac{\int 2\pi b\, db\, I_b(\infty)\, e^{-I_b(\infty)}}{\int 2\pi b\, db(1-e^{-I_b(\infty)})}\,, \tag{14}$$

where $I_b(\infty)$ is the integral of $\sigma\rho$ along the straight-line trajectory through the entire nucleus at impact parameter b [see Eq. (2)]. At 100 MeV, F is close to $\frac{1}{5}$ for Pb and to $\frac{1}{3}$ for Ca. It becomes larger at lower energies.

Although the effects on the reaction cross sections of the Coulomb plus nuclear fields (by way of changes in the pion's kinetic energy) are not very large for positive pions, they can be as large as 30% or more for negative pions where the two effects act in the same direction.

6. The effect of the nucleon momentum distribution

So far, in our estimates of the pion-nucleus reaction cross section, it has been assumed that the target nucleons are at rest. The momenta of nucleons in nuclei are however comparable to those of the incident pions. Although the average momentum $\langle p\rangle$ of these nucleons vanishes, the average square $\langle p^2\rangle$, does not. As a result the mean kinetic energy of the π-nucleon relative motion necessarily exceeds the kinetic energy of the incident pion. Because of the strong dependence of the π-nucleon cross section on energy, we must estimate the possible magnitude of this relative energy shift on the cross section.

If p_0 is the momentum of a pion incident on a nucleon of speed V, and p_0' is the corresponding momentum in a frame where the nucleon is at rest, then for an array of isotropically moving nucleons

$$\langle (p_0')^2\rangle = p_0^2\left\{1+\left[\frac{V}{c}\right]^2\left[\frac{4}{3}+\left[\frac{m_\pi c}{p_0}\right]^2\right]\right\}, \tag{15}$$

where m_π is the pion rest mass. For a 100 MeV pion and a nucleon speed ($\beta\approx 0.15$) characteristic of nuclear matter, the value of the curly brace corresponds to an increase of the average pion kinetic energy of about 6%. This would in turn imply an increase of the pion-nucleus cross section of about the same size.

Actually, the cross section corresponding to the average collision energy somewhat underestimates the average cross section for a distribution of nucleons because of the strong upward curvature of the π-nucleon excitation function in the energy region near 100 MeV. That is, the high-relative-energy encounters increase the average cross section more than the low-relative-energy encounters reduce it. On the other hand, the cross sections are somewhat reduced from our original estimate (in which nucleon motion was neglected) by Pauli blocking. Overall, the effect of taking into account the nucleon motion and the Pauli principle is not very large, although it is not altogether negligible.

We are in a position to review where we stand on the prediction of the reaction cross sections. Table III lists the measured reaction cross sections for three target elements (C, Ca, and Pb) for 100 MeV positive pions along with the model estimates for the same three cross sections. The only feature of the latter estimates which goes beyond the use of straight line classical trajectories and free π-nucleon cross sections is the inclusion, in the column labeled σ_{cC}, of the effect of refraction in the Coulomb field of the nucleus (effect 1 of Sec. V A 1). The table shows that these model cross sections for all three targets are only about 0.77 times as large as the measured cross sections. We have just examined a number of considerations which had *not* been included in the model estimates of Table III, but could nevertheless affect the size of the pion reaction cross sections.

The largest such effect for positive pions ($\sim 10\%$) was that due to the refraction of the trajectories in the nuclear force field. The effect of the Coulomb plus nuclear potentials on the pion kinetic energy could increase the cross section in light nuclei up to 10 percent. The effect in heavy nuclei would be smaller. The effects associated with the range of the pion-nucleon force, the pion wavelength, and the motion of the nucleons are all probably smaller than the first two effects mentioned. Some of these effects are less certain than others, but taken together, they seem to bring the magnitude of estimated cross sections into adequate agreement with the measurements, considering the uncertainties of both.

B. The A dependence of the π^+ reaction cross sections

It is easy to appreciate that cross sections represented by Eq. (4) must increase at a rate between $A^{2/3}$ and A for a set of nuclei which are "similar in shape," but differ in size. (Two nuclei are similar in shape when the density of one at radius vector $\mathbf{r}$ is the same as that in the second at $\lambda\mathbf{r}$ where λ is a scaling factor.) Where nuclei are relatively transparent to a projectile, the dependence is closer to A; where they are opaque (as for pions) the dependence is closer to $A^{2/3}$. Nuclei which are described by a Woods-Saxon density function, with a fixed diffusivity for all nuclei, are not similar in shape because the ratio of radius to edge thickness varies with A. This makes the amount of shadowing in heavy nuclei larger than it would be if they were similar in shape to light nuclei. It leads to a slight reduction of the exponent in the A dependence. The cross-section ratio between Pb and Ca actually calculated according to Eq. (4) is consistent with these considerations. These cross sections are given in the fourth column of Table III and vary as $A^{0.65}$ at 100 MeV. The Coulomb refraction factor is taken into account in the fifth column of Table III and reduces the A dependence between Ca and Pb to $A^{0.58}$. The effect of the Coulomb field on the pion's kinetic energy together with the energy dependence of the reaction cross section reduces the ratio of Pb to Ca cross sections by only 3% and the A-dependence exponent by 0.01. Altogether then one would expect an A dependence between Ca and Pb of roughly $A^{0.57}$. The measured A dependence of the reaction cross sections (third column of Table III) in the same mass range is $A^{0.57}$, in excellent agreement with expectations.

C. The ratio of π^- to π^+ reaction cross sections

Another useful comparison is that between positive and negative pions incident on the same nucleus. According to the earlier discussion, there should be three main differences between the calculations of π^+ and π^- reaction cross sections for a heavy nucleus. (We emphasize heavy nuclei because it is here that the $\pi^\pm$ cross sections would be expected to differ most. In light nuclei since $Z \cong N$, the reaction cross sections should be very nearly equal.)

(i) In Pb, the mean pion-nucleon interaction cross section should be about 20% larger for π^- than for π^+ as a result of the greater number of neutrons than protons in the nucleus and the fact that π^- (π^+) reacts predominantly with neutrons (protons) at the energies considered. According to our earlier estimates a 20% excess in the π^--nucleon cross section should lead, at 100 MeV, to about a 4% greater reaction cross section for π^- than π^+.

(ii) The Coulomb field refraction also enhances the π^-/π^+ cross-section ratio, roughly by the factor $(1+V_C/T_\pi)^2$ which for Pb at 100 MeV is about 1.35. This is the largest effect.

(iii) The third effect is due to the different kinetic energies in the nuclear surface region of positive and negative pions which have the same incident energy. Assuming that any changes in kinetic energy due to *nuclear* forces are the same for π^+ and π^- (the optical potentials are very similar[26]), the kinetic energy difference arises entirely from the *Coulomb* forces. For Pb, this difference is about 30 MeV, leading to a factor of about 1.2 in the ratio of expected π^- to π^+ reaction cross sections.

Because the foregoing π^-/π^+ enhancement factors for the three effects are not uncorrelated, it is probably not legitimate to simply multiply them together. Nevertheless, the rather substantial value of their product, ≈ 1.7, tells us that at 100 MeV one should expect a much greater ratio of π^- to π^+ reaction cross sections in Pb and other heavy elements than in light nuclei. This is in accord with the expectations of optical models which fit elastic cross sections and other data.[27]

The sum of the absorption plus charge exchange cross sections has been measured by Ashery *et al.*[6] for a number of nuclei with both π^+ and π^- at 125 MeV. If we add the value of our π^+ inclusive inelastic scattering cross section, extrapolated to 125 MeV, to this result, we should have a reasonable estimate for the total π^+ reaction cross section at 125 MeV. To obtain a corresponding value for the π^- cross section (for which we do not have inelastic data), we add to their π^- charge exchange plus absorption results, our π^+ scattering cross section (extrapolated to 125 MeV) multiplied by their ratio of N_{eff} values for π^- and π^+. In any case, the ratios of π^- to π^+ *reaction* cross sections so obtained are not very sensitive to the size of the inelastic scattering component since it constitutes a relatively small part ($\sim\frac{1}{4}$) of the reaction cross section. The resulting "measured" ratio of the π^- to π^+ reaction cross sections for Pb or Bi at 125 MeV turns out to be only 1.1. (The fact that the data were obtained at 125 MeV while most of our considerations were for 100 MeV should not make much difference.) And although the cited uncertainties of the measured absorption plus charge exchange cross sections are fairly large ($\sim$20%), one must, at least tentatively, regard the discrepancy as serious.

This experimental result is consistent with the ratio 1.24 obtained from a comparison of π^- to π^+ induced spallation yields in Au at 100 MeV (Table VI of Ref. 25). There are however considerable uncertainties about the π^-/π^+ cross-section ratio in this spallation study because the yield patterns differ considerably where ΔZ or ΔN are small and it is here that the cross sections are large.

Both these results are disconcertingly smaller than the π^-/π^+ ratio which one would expect on the basis of the foregoing considerations. In particular, the two Coulomb effects on the π^-/π^+ ratio seem hardly to be questioned since they are independent of the interaction mechanisms. The first effect (responsible for a factor of 1.4) comes from refraction in the Coulomb field before the pion even gets to the nucleus. The second (introducing a factor of about 1.2) is due to the higher kinetic energy of the π^- than the π^+ when it reaches the nucleus, combined with the strong energy dependence of the π-nucleon cross section. The fact that the observed energy dependence of the π-nucleus 180° cross section can be accounted for in terms of that of pions on free nucleons (see Sec. VI A below) makes it unlikely that this second Coulomb factor can be ruled out. One must therefore be puzzled by the failure of the model calculation, and of related cascade calculations,[25] to reproduce the small π^-/π^+ ratios of reaction cross sections which have been deduced from measurements.

VI. THE INTERPRETATION OF THE $(\pi^+,\pi^{+\prime})$ DIFFERENTIAL CROSS SECTION IN TERMS OF THE MODEL

In this section we will use Eq. (8) to estimate the magnitudes, A dependences, and energy dependences of the 180° cross section for comparison with the results of our measurements. The latter are summarized in Fig. 12 and in Table IV.

To carry out numerical integrations of Eq. (8) it is necessary to specify an explicit form for the branching ratio D. We write $D=\Gamma_d/(\Gamma_d+\Gamma_r)$, where Γ_d is the width for the initially formed π-nucleon complex to decay back into a pion plus a nucleon and Γ_r is the width for the removal of the complex from the quasielastic channel. This removal occurs whenever the complex has some interaction with a nuclear constituent. Γ_d includes decay into neutral as well as into charged pions when such decay is possible. Γ_r includes scattering as well as true pion absorption by nuclear particles.

It is reasonable to assume that the removal width (sometimes called the spreading width), Γ_r, is proportional to the local nucleon density. Γ_d, on the other hand, can be assumed to be independent of the local density. (Although it is true that Pauli blocking can reduce the value of Γ_d from that in free space, its effect is small for 180° scattering.) We may therefore write

$$D=\frac{1}{1+\alpha\rho/\rho_0}\ , \tag{16}$$

where ρ_0 is the central nucleon density and α is the value of the ratio of Γ_r to Γ_d at this density. The constant α may, in principle, depend on the initial pion energy and on the ratio of neutrons to protons in the nucleus. However one should not expect Γ_r to change very rapidly with energy since it describes the behavior of the interaction cross section between the π-nucleon complex and another nucleon. It should behave like a nucleon-nucleon cross section. For similar reasons, Γ_r may also not be very isospin dependent although its partition into a rescattering width and a true-pion-absorption width is definitely sensitive to isospin. Since little is actually known about the magnitude or dependences of the constant α, the integrations of Eq. (8) were carried out for a number of different values for this parameter.

TABLE IV. Measured[a] 180° π^+ differential cross sections (mb/sr) at three energies (laboratory coordinates).

	67 MeV	85 MeV	100 MeV
C	15±2	23±2	25±2
Ca	30±4	43±5	50±5
Sn	38±5	52±6	69±7
Pb	48±7	61±7	84±8

[a]See footnote to Table I.

The integrand of Eq. (8) is proportional to the number of pions in an incident beam which have their first interaction at location (z,b) in the target nucleus. This probability has been plotted as a function of z for several values of the impact parameter b in Fig. 13. It is seen that the first pion-nucleon encounters occur mainly in the nuclear surface.

In comparing model calculations with observed differential cross sections, we will focus on the data for Ca and for Pb at both 67 and 100 MeV. The results of the integrations of Eq. (8) for these particular examples are given in Table V for three choices of α (0, 1, and 2). The cross sections listed in the table are not simply the integrals of Eq. (8). In addition they include both of the Coulomb corrections which have already been mentioned in connection with the reaction cross sections. The corrections at 67 MeV for the refraction of the pions in the Coulomb field of the target nucleus reduce the cross section of Eq. (8) by 12% for Ca and 26% for Pb. At 100 MeV these corrections drop to 7% and 16%, respectively. The corrections associated with the kinetic energy change of the pion in the Coulomb field of the target are 14% and 27% for Ca and Pb at 67 MeV and 7% and 14% at 100 MeV. The size of the kinetic energy corrections depend only slightly on the choice of the value for α. The values given above are for $\alpha=1$.

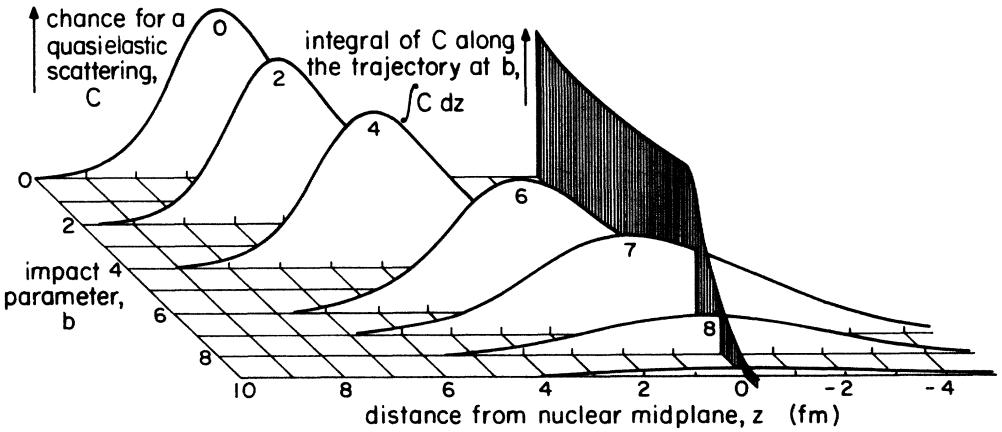

FIG. 13. The calculated contributions to the 180° scattering cross section according to Eq. (8) for Pb at 100 MeV. These contributions are plotted as a function of the distance z of the incident pion from the midplane of the target for a number of impact parameters, b. The shaded curve in the midplane is proportional to the total contribution to the cross section as a function of impact parameter. For the particular calculations shown in the figure the decay parameter α was set equal to zero. The scattering probabilities are however not very sensitive to the value of α.

TABLE V. 180° π^+ differential cross sections according to Eq. (8).[a]

Assumed value[b] of α	Target	$d\sigma/d\Omega$ (mb/sr) at 67 MeV	$d\sigma/d\Omega$ (mb/sr) at 100 MeV
0	Ca	24	40
	Pb	46	84
1	C	7	14
	Ca	16	29
	Sn	25	47
	Pb	29	57
2	Ca	13	24
	Pb	22	45

[a]These calculated cross sections include the correction factors due to the incident pion's refraction and decrease in energy in the Coulomb field of the target nucleus.
[b]α is the branching parameter defined in Eq. (16).

A. Magnitudes of the 180° scattering cross sections

If one compares the Coulomb-corrected differential cross sections of Table V with the measured cross sections (Table IV), it is seen that they are too low for any reasonable value for α. Although the agreement is not too bad for $\alpha=0$, values of α much below unity are unacceptable because they would not provide for enough pion absorption. Pion absorption is well known to constitute the bulk of the reaction cross section.

Just as the repulsive Coulomb field acts to reduce the π^+ cross sections, the attractive nuclear potential acts to increase them. The effect of the nuclear potential can also be broken into two factors, one due to refraction and the second due to the pion's change in kinetic energy. These have been discussed in connection with the reaction cross section in Sec. V A 4 and in Appendix C. The refraction effect increases the differential cross sections by about 10%. Estimates for the effects of the pion's energy shift in the nuclear potential lead to an increase in the cross section by a factor of 1.6 for Ca and 1.5 for Pb at 67 MeV. The corresponding factors at 100 MeV are 1.3 and 1.2. When the cross sections in Table V are corrected for both the refraction and kinetic energy effects of the nuclear potential they become (for the choice $\alpha=1$): 67 MeV (Ca: 28 mb/sr, Pb: 48 mb/sr) and 100 MeV (Ca: 41 mb/sr, Pb: 75 mb/sr). These cross sections are in good accord with the measured ones (Table IV) at 67 MeV and are slightly low at 100 MeV. They would be somewhat improved overall, if a modest correction of the measured cross section is made for multiple scattering.

The Coulomb field corrections which led us to reduce the cross sections computed from Eq. (8) are hardly open to controversy. The corresponding nuclear field correction for the effective pion energy which was discussed in the preceding paragraph is, however, much less certain. It seems clear, nevertheless, that some upward correction of Eq. (8) is needed if one is to account for the observed scattering cross section in terms of the free-nucleon cross sections. Although one might imagine that processes which are not included in the formulation behind Eq. (8) can contribute to the observed cross section, the fact that the angular distributions are backward-peaked speaks for quasielastic scattering from nucleons as the major scattering process. To see whether the quasielastic cross section would be significantly increased due to effects of the Fermi motion of the nucleons we carried out a number of exercises. They show that when the effects of Pauli blocking are included, the overall effect on the cross section is small. It would appear that only the nuclear potential, among all of the factors considered, seems capable of providing the appreciable upward correction to the calculated cross section which is needed.

B. The energy dependence of the 180° $(\pi^+,\pi^{+\prime})$ cross section

It was seen in the preceding exercise that, with both the nuclear and Coulomb field corrections, the model cross sections change between 67 and 100 MeV by a factor of $\frac{41}{28}\sim 1.5$ and $\frac{75}{48}\sim 1.6$ for Ca and Pb, respectively. Considering the uncertainties in the data and in the model estimates, these results are in good agreement with the ratios (~ 1.7 for both Ca and Pb) of the observed cross sections listed in Table IV.

It is easy to appreciate why this ratio is so much smaller than the corresponding ratio, 2.7, for pion-proton scattering (in the laboratory frame). Although the contributions to 180° scattering for large impact parameters on nuclei are expected to show the same energy dependence as the pion-nucleon $d\sigma/d\Omega$, at small impact parameters they should track with the ratio

$$S=(d\sigma/d\Omega)/(\sigma_{\text{in}}+\sigma_{\text{out}})\ .$$

This ratio actually *decreases* slightly with increasing incident energy because the π-nucleon angular distribution happens to be slightly less backward peaked at 100 MeV then it is at 67 MeV. Thus, when Eq. (8) is integrated over all impact parameters, the low impact parameter contributions reduce the steepness of the energy dependence.

C. The A dependence of the 180° $(\pi^+,\pi^{+\prime})$ differential cross sections

The calculated cross-section ratios Pb/Ca in subsection B are $\frac{48}{28}\sim 1.7$ at 67 MeV and $\frac{75}{41}\sim 1.8$ at 100 MeV. These ratios correspond to mass-number dependences going as $A^{0.32}$ and $A^{0.36}$, respectively. Our observed dependence is $\sim A^{0.30\pm 0.06}$ at both energies. At 125 MeV, the data of Ashery *et al.*[6] go as $A^{0.34}$ for π^+ when they are expressed in terms of A. It appears that the model, with corrections for the effects of Coulomb and nuclear potentials, is within reasonable range of the observations. The A dependences of the model are rather insensitive to the assumed value for α.

The A dependences as well as other features of the cross sections are shown to arise from the convolution of several independent factors, each responsible for only a relatively small part of the observed dependence. The fact that the differential cross section goes very nearly as $A^{1/3}$ is not to be accounted for simply in terms of some spatial dependence (e.g., that $A^{1/3}$ represents some relevant length in the nucleus).

There are a number of reasons that the A dependence of the differential cross section is weaker than that of the reaction cross section. One reason has to do with the role of the factor $(d\sigma/d\Omega)/(\sigma_{in}+\sigma_{out})$ in Eq. (8). There is no such factor in Eq. (4) for the reaction cross section. This factor decreases between Ca and Pb because $d\sigma/d\Omega$ for π^+ tends to be proportional to Z whereas the σ's also depend on N. The ratio of Z to N falls from unity to $\sim\frac{2}{3}$ in going from Ca to Pb.

D. The ratio between normal and charge exchange backward-scattering cross sections

It is useful to compare charge exchange and normal quasielastic scattering because they should be closely related. The interaction mean free path for a positive pion entering a nucleus is the same whether it eventually scatters with or without charge exchange. In short, we could write an equation virtually identical to Eq. (8) for quasielastic charge exchange scattering. The ratio of the $\pi^+\rightarrow\pi^0$ to $\pi^+\rightarrow\pi^+$ quasielastic cross sections would be simply N/Z times r, the ratio of the charge exchange to the normal scattering π-nucleon cross section. [We are ignoring the contribution of the neutrons to the 180° normal scattering of π^+ because it is negligible (Table II).]

Very recently Ashery *et al.* have measured the charge exchange (cx) cross sections for several nuclei at 160 MeV.[28] These new results can be compared with earlier measurements[6] of the normal quasielastic scattering cross sections at the same energy. In the notation of these authors, the ratio of the two measured cross sections is $(N_{eff})_{cx}/(N_{eff})_{norm}$ times r. It follows that their ratios of N_{eff} (cx to normal) should be equal to simply N/Z for π^+ and to Z/N for π^-. The measured N_{eff} values for charge exchange[28] and normal[6] scattering for Pb (or Bi) are

	cx	normal	ratio (cx/norm)
π^+	6.6	4.3	1.5
π^-	3.1	5.3	0.6

For Pb, the ratios in the last column are expected to be $N/Z=1.5$ for π^+ and $Z/N=0.7$ for π^-. The agreement is very good. The same authors also provide N_{eff} data for carbon. Here the values are

	cx	normal	ratio (cx/norm)
π^+	1.6	1.4	1.1
π^-	1.6	1.3	1.2

The expected ratios (Z/N and N/Z) are both equal to unity. The overall level of agreement in these simple comparisons can be taken as support for the assumptions which underlie Eq. (8). However, it must be pointed out that we have here ignored possible Coulomb effects on the *outgoing* charged pions. We have also implicitly assumed that the average D factors of Eq. (8) are equal to each other for all Δ complexes (Δ^-, Δ^0, Δ^+, and Δ^{++}) that are involved in the four scatterings which are being compared.

E. The comparison of the 180° cross sections for π^+ and π^-

We were not able to measure the spectra and angular distributions for negative pions with our telescope and will therefore compare the model predictions for the rate of π^+ and π^- yields in backward directions with measurements of Ashery *et al.*[6] They obtained single-arm pion yields and angular distributions (but not spectra) at several incident energies using a pair of plastic scintillators in a telescope. They find, at 125 MeV, that for light elements the π^+ and π^- scattering cross sections in the back hemisphere are very nearly equal. The π^- to π^+ cross-section ratio rises steadily with A reaching ~ 1.2 for heavy elements.

Before we compare these results to the predictions of the model, we must mention the results[29] of Piasetzky *et al.* on the comparison of the (π^-,π^-n) with (π^+,π^+p) reactions at 165 MeV. In these coincidence experiments, the cross-section ratio $(\pi^-,\pi^-n)/(\pi^+,\pi^+p)$ was found to be unity (to within 10%) for carbon, and to increase very rapidly with A, reaching a value of over 3 for Bi. These results are not, strictly speaking, directly comparable to the single-arm results of Ashery or ourselves since they involve additional interactions. For example the probability for the proton in (π^+,π^+p) to successfully escape from a nucleus is expected to be somewhat less than that for the neutron in (π^-,π^-n). Nevertheless, the considerable difference between the Ashery single-arm π^-/π^+ ratio and the corresponding coincidence ratio of Piasetzky is not easy to understand. In a model calculation[29] in which he attempts to account for this difference on the basis of differing radii for the neutron and proton distributions in the nucleus, Piasetzky underestimates his own measured ratio by 20% and overestimates Ashery's by the same amount. It may be reasonable to conclude that one should regard the various experimental π^- results as somewhat less well established than the π^+ results.

For the single-arm π^-/π^+ ratio in Bi at 100 MeV our classical model gives an expected value of 2.4. This is for calculations which include Coulomb field corrections and where α is set equal to unity. (The predicted ratio is very insensitive to the assumed value for α.) This prediction may be legitimately compared to the Ashery measurements at 125 MeV because both the observed and calculated π^-/π^+ ratios change very slowly with incident energy. The predicted ratio can be broken down into three factors: (1) Equation (8) (which does not include Coulomb effects) provides a factor of 1.25 favoring π^-. [It comes mainly from the factor $(d\sigma/d\Omega)/(\sigma_{in}+\sigma_{out})$ and is associated with the neutron excess in heavy nuclei.] (2) The refraction in the Coulomb field of the nucleus is responsible for an additional factor of 1.4. (3) Finally there is the effect of the increase (and reduction) of the π^- (and π^+) kinetic energies in the nuclear surface when they have the same incident energy. This gives a factor of ~ 1.35. There is presumably no net effect due to the pion-nuclear potentials. They appear to be much the same for π^+ and π^-.[26] The discrepancy between the model prediction, 2.4, for the π^-/π^+ ratio, and the measurement, 1.2, of Ashery *et al.* becomes even larger if one assumes in the model that neutrons stick out farther than protons in heavy nuclei.[29]

There are however two additional Coulomb effects which have not yet been taken into account. They do not bear on the reaction cross sections, but may affect the scattering cross sections because they involve the pions on their way *out* of the nucleus.

The first effect is the refraction of the emerging pion in the nuclear Coulomb field. The outgoing pion has less energy than the incident pion and since the refraction correction goes inversely as the pion energy we cannot ignore a possible effect on outgoing pions, having found one for the incident pions. The Coulomb field deflects positive pions in the radial direction and negative pions toward the tangent plane at the emission point. This is likely to enhance the 180° emission of π^+ somewhat and decrease the corresponding yield for π^-. The effect is probably not very large since the maximum deflection angles are $\sim V_C/2T_\pi$ (only about 8° for a 50 MeV pion escaping from a Pb nucleus). The success of the comparison of normal (charged) scattering with single charge exchange scattering of subsection D, carried out without taking outgoing Coulomb effects into account, provides some reassurance that these effects are not very large.

The second effect of the Coulomb field on the outgoing pion relates to its *energy* spectrum. The nuclear potential combined with the Coulomb potential may affect the energies of outgoing pions very differently in π^+ and π^- scattering. The effect can be made clear with the help of Fig. 14 which shows the relevant kinematics. The curves give the outgoing pion energy as a function of incoming energy for scattering from a stationary nucleon at three laboratory angles in the back hemisphere.

Consider first a positive pion of 125 MeV incident on a Pb nucleus. If we make the assumption that the local value of the optical potential can be used to estimate the mean kinetic energy of the pion, then this pion will have about 130 MeV of kinetic energy at the typical collision site in the surface of the Pb nucleus. (It picks up 20 MeV due to the nuclear attraction and loses 15 MeV from the Coulomb repulsion.) This is, overall, a small energy change and the pion therefore emerges on scattering with much the same energy, ~57 MeV, that it would have if the Coulomb and nuclear fields had been turned off.

It is different for a negative pion of the same incident energy for here the nuclear and Coulomb fields are both attractive. At the collision site, the energy of such a pion is $125+15+20=160$ MeV. From Fig. 14 this pion would recoil to 180° with 70 MeV. On the way out, it must, however, return the "borrowed" 35 MeV and so it emerges with only 35 MeV. At 100 and 85 MeV incident energies, the π^- emergence energy would drop as low as 26 and 20 MeV, respectively.

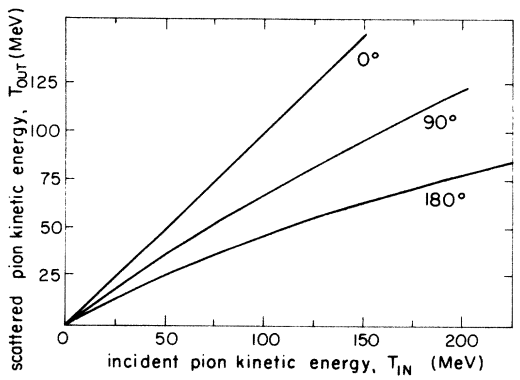

FIG. 14. The outgoing laboratory energy of a pion scattered from a stationary nucleon as a function of the incident pion energy for three scattering angles.

This effect is simply due to kinematics. It arises from the fact that the slope of the curve for T_{out} vs T_{in} is significantly less than unity at backward angles for π-nucleon scattering. (It is also relevant that the fields responsible for the energy changes are not those from the pion's collision partner but are provided by a third body, the nucleus as a whole.)

Although the π^- emission energy at an incident energy of, say, 85 MeV will be higher at other emission angles than the 20 MeV which applies at 180°, it must be kept in mind that the struck nucleons are not at rest and that as a result, the outgoing pion spectra are broadly spread around the central energy which one would estimate for initially stationary nucleons. Some negative pions may in fact be emitted with less than the necessary escape velocity and, of those which do escape, a fair number may have too little energy to pass the acceptance criteria of pion detectors. These particular effects are consequences of the (uncommon) negative charge of these pions. To estimate the magnitudes of these effects it would be helpful to know the shapes of the π^- spectra better than we currently do. It is possible that the Coulomb effects on outgoing pions may account for a part of the discrepancy between prediction and observation of the π^-/π^+ differential scattering ratios. They do not, however, bear on the problems with the π^-/π^+ ratios of the reaction cross sections.

To summarize this discussion of π^-/π^+ ratios: the model predictions are definitely in disagreement with the magnitude of the π^-/π^+ ratio measured by Ashery *et al.* for heavy elements. They are consequently also in disagreement with the A dependence for $(\pi^-,\pi^{-'})$ of these observations. However because of the very large ratios observed by Piasetzky in the corresponding coincidence measurements and because of the uncertainties in some of the possible Coulomb effects, it is not clear how concerned one should be at this time about these discrepancies.

VII. SUMMARY AND CONCLUSIONS

In this paper we have reported the result of a survey of the inclusive scattering of positive pions from nuclei at incident energies from 67 to 100 MeV. The pion detector, a multicrystal intrinsic germanium telescope, provided full-range spectra with an energy resolution of about 2 MeV. The detector was able to distinguish pions from muons and other particles at all angles back of 50°. The identification of pions was considerably more difficult at forward angles (as it is also for other types of detectors in similar measurements). Fortunately the forward pion scattering cross sections are small and do not contribute significantly to the overall inclusive scattering. Angular distributions of the integrals of the spectra were obtained for four

targets at three incident energies, and by integrating these distributions, the total inclusive $(\pi^+,\pi^{+'})$ cross sections were determined at these three energies.

In analyzing the results we were mainly concerned with the dependence of the measured cross sections on incident energy, on the target mass, and (using the data of others) on the sign of the incident pion. These features of the data for the total reaction cross sections and for the quasielastic differential cross sections can be identified with the very first interaction of the pion in the nucleus. For pions (uniquely among the common strongly interacting projectiles) a large fraction of the scattered particles have only a single interaction in the nucleus. One should therefore be able to treat the data associated with these single initial interactions with more confidence than one would be able to treat data which involve subsequent interactions of the pion and its collision partners in the target nucleus. It was therefore decided to limit the analysis in this paper to those features of the data which are related to the first collision. (Aspects of the data which refer to the full nuclear cascade have been studied separately using Monte Carlo techniques. This analysis will be reported in a forthcoming paper.[30])

Two features of the data which do refer to the first collision have been dealt with only qualitatively in this paper because they depend sensitively on the (somewhat uncertain) effective momentum distribution of struck nucleons. These features, the detailed shapes of the energy spectra and of the pion angular distributions, can best be dealt with using Monte Carlo techniques.[30] By and large the spectral shapes seem consistent with the assumption of a standard momentum distribution for the target nucleons. At back angles the quasielastic spectra are however so wide that they are not sufficiently distinguishable from a possible multiple-scattering background to allow one to use the spectral shapes to estimate a magnitude for this background.

Some of the measured spectra show structures which are associated with the excitation of giant resonances. The extraction of the strengths and angular distributions of these resonances is unfortunately hindered by the pervasive background of quasielastic scattering.[31]

The inclusive scattering data were examined in terms of a simple classical model which provides a framework for the consistent comparison of various types of measurements. There are two major ingredients in the model. The first, having to do with the purely geometrical aspects of the reactions, determines the distribution of the sites of the pion's first interaction in the nucleus. The second ingredient deals with the nature and characteristics of the interactions which occur at these first-collision sites. The viewpoint taken in the present paper starts with two basic assumptions about the nature of the interactions. (1) All pion interactions in the nucleus start with a pion's involvement with a single nucleon. If there is no further interaction, the π-nucleon complex thus formed soon decays giving rise to an event which is interpreted as a quasielastic scattering. (2) The parameters of this quasielastic scattering (i.e., size of cross section, angular distribution) are the same as they would be for a pion of appropriate kinetic energy colliding with a free nucleon. There is one free parameter in the model, that giving the probability that the π-nucleon complex has a further nuclear interaction before it can decay.

Model predictions of various cross-sections ratios were compared with corresponding measured ratios. (Both the model predictions and the measurements can be better trusted for ratios than for values of absolute cross sections.) It was felt at the start that any serious discrepancies between model predictions and the data would probably indicate some failing in the assumptions about the nature of the pion's interaction in the nucleus, since it seemed unlikely that the geometrical component of the prediction could be seriously misestimated.

There is a small measure of arbitrariness in the assumption that all initial interactions begin with only a single nucleon, but not much. Calculations in which a competitive absorption branch can occur in parallel with the option for a quasielastic collision turn out not to differ very much from the calculations with the assumed model.

The results of the comparison of predictions with data were briefly as follows: For the π^+ reaction cross sections, the magnitudes of the cross sections and their observed A dependence were reasonably well accounted for. The model, however, predicted a higher-than-observed ratio for π^-/π^+ reaction cross sections in heavy nuclei. For the 180° differential scattering cross sections, the model correctly gave the observed energy dependence of the π^+ cross section and reasonably accounted for the ratio of charge exchange to normal scattering. It gave a reasonable account of the magnitudes and A dependences of the differential cross sections if it was assumed that the effective pion kinetic energy in the nuclear surface could be estimated from the local optical potential. It may again have overestimated the π^- cross sections with respect to the π^+ cross sections, but the available data here are conflicting.

All in all the general agreement between the model implications and the available data appears to be good enough to suggest that the model assumptions are not far from the truth, that is, that π-nucleon interaction parameters *inside* the nucleus do not differ substantially from the free π-nucleon parameters. One is therefore encouraged to take seriously any persistent discrepancies between the model and observations. It would appear from our analysis, that careful comparative measurements of π^- vs π^+ spectra and angular distributions might help clarify some of the uncertainties in applications of the model.

ACKNOWLEDGMENTS

We would like to express our appreciation to Professor L. Knutson, Dr. M. D. Cooper, and Dr. J. Sherman who helped get this experimental survey underway and to professor G. A. Miller and Professor L. Wilets for helpful conversations. We are grateful to Dr. T. Murakami for helpful comments on this manuscript. The steady support from the staff at LAMPF is gratefully acknowledged. This work was supported by the Department of Energy.

APPENDIX A: THE EFFECT OF THE PION-NUCLEON INTERACTION RANGE ON THE REACTION CROSS SECTION

The effect of the range of the pion-nucleon interaction was neglected in the derivation of Eq. (4). Suppose that $\mathscr{R}$ represents this range in the sense that if a pion passes within a distance $\mathscr{R}$ from the center of a nucleon, it is sure to interact, and that if it passes at a larger distance, it is sure not to interact. Then the quantities $I_b=\sigma\int\rho\,dx$ in Eq. (4) should be replaced by quantities $\bar{I}_b=\sigma\int\bar{\rho}\,dx$ where $\bar{\rho}$ is the average value of ρ at (x,b) in a disc of radius $\mathscr{R}$ perpendicular to the beam and centered on the trajectory at b.

There is nothing very general that can be said about the effect on the cross section of this smearing of the effective nucleon density distribution, because the effect depends on the magnitude of σ as well as on the density distribution. For example if the nucleus were shaped like a soup can of radius R lined up with the beam and contained a uniform density of nucleons, then the reaction cross section would approach $\pi(R+\mathscr{R})^2$ in the limit where the projectile path through the cylinder is very many mean free paths long. This model is, however, inappropriate for nuclei because of its sharp discontinuity of density at the nuclear edge. The projected density of an actual nucleus in the plane perpendicular to the trajectories changes gradually with b because of the nuclear shape (a sphere rather than a cylinder) and because of the nuclear diffusivity. The results of simple exercises comparing the integrals [Eq. (4)] of $1-\exp(-\bar{I}_b)$ with those of $1-\exp(-I_b)$ show that for realistic densities the effects on the cross section of the introduction of a reasonable pion-nucleon force range are relatively small ($\lesssim 5\%$).

APPENDIX B: THE EFFECT OF THE PION WAVE LENGTH ON THE NUCLEAR REACTION CROSS SECTION (IN THE ABSENCE OF A REAL NUCLEAR POTENTIAL)

To investigate possible differences between the wave-mechanical and classical reaction cross sections for the same scatterings, we began with a set of simple comparison exercises. First classical cross sections were calculated using Eq. (4) for assorted combinations of the critical parameters: (i) σ, the interaction cross section of the projectile with a typical target nucleon and (ii) the parameters relating to the distribution of nucleons in the nucleus. For the latter, Woods-Saxon distributions were assumed. Each classical calculation was followed by a corresponding wave mechanical calculation *with the same parameters*. Here the incident particles were represented by plane waves (corresponding to classical straight-line trajectories) and their scattering was handled nonrelativistically. The potential in these calculations was purely imaginary (since there is no real potential in the corresponding classical calculation). The value of this imaginary potential, W, as a function of position in the nucleus was taken to correspond to the local mean free path, Λ, of the corresponding classical problem. The explicit connection between W and Λ is given by

$$\frac{W}{T}=\frac{\lambda\!\!\!^{-}}{\Lambda}\left[1+\frac{1}{4}\left[\frac{\lambda\!\!\!^{-}}{\Lambda}\right]^2\right]^{1/2},$$

where T is the projectile kinetic energy and $\lambda\!\!\!^{-}$ is its corresponding wavelength.

In exercises where the parameter values were chosen to match those appropriate to pion scattering from Ca and Pb at 67 and 100 MeV, the classically and quantum-mechanically calculated cross sections were found to agree within a few percent.

It is instructive to compare the actual contributions to the cross section as a function of the impact parameter, b (for the classical calculations), with those for the corresponding orbital momentum, l (for the wave calculations). The relation between these quantities is $b=(l+\frac{1}{2})\lambda\!\!\!^{-}$. A plot of the classical interaction probability function $T_b=1-\exp(-I_b)$ is given in Fig. 15 as a function of b for a set of parameters corresponding to 100 MeV pions on Pb. Also plotted are the corresponding wave quantities $1-|\eta_l|^2$ obtained from the wave calculations for integral values of l. Here η_l, as usual, gives the outgoing amplitude of the lth wave. For both calculations the interaction probabilities are very close to unity at small b and l. The wave calculation undershoots the classical calculation at the knee of the probability curve and overshoots it in the tail. This is qualitatively what one would expect if the wave solution represents a measurement of the classical probability function with a probe of resolution $\sim\lambda\!\!\!^{-}$.

The important point is that the cross section calculated in terms of a wave picture exceeds only slightly that cal-

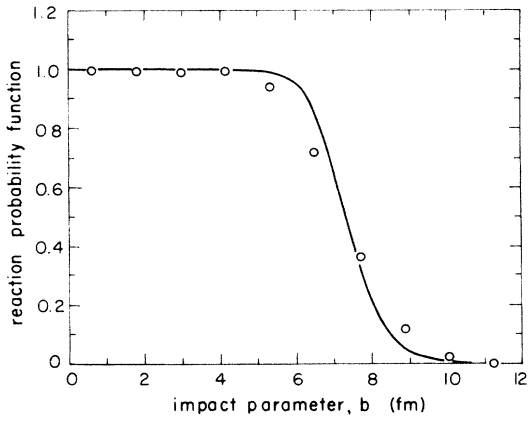

FIG. 15. The curve gives the classically calculated probability per unit projected area for the scattering of 100 MeV pions from Pb as a function of impact parameter. The points give the results of a corresponding plane wave calculation (see the text) where the partial waves are associated with classical impact parameters according to $b=(l+\frac{1}{2})\lambda\!\!\!^{-}$.

culated classically. The wave-calculated result is not related to the classically calculated result by the addition of $\lambda\!\!\!^{-}$ to the classically determined R_p where πR_p^2 is the classical cross section. [For Ca at 67 MeV $\pi(R_p+\lambda\!\!\!^{-})^2$ would be almost twice as large as πR_p^2 but the wave-calculated cross section is actually only a few percent larger than the classical πR_p^2.]

In fact if the potential was allowed to change more abruptly than it does in the present exercise (with Woods-Saxon shapes) there would be wave reflection from the nuclear surface in the quantum-mechanical calculation and this would reduce the quantum cross section below the classical one.

We should not leave this discussion without remarking on the prevalent use of the expression $\pi(R+\lambda\!\!\!^{-})^2$ for fast neutrons and other projectiles. It is shown in Appendix C that when an attractive real potential is present it gives rise to refraction effects which increase the cross section from the value, πR_p^2. This occurs both classically and in wave mechanics. The reason that fast neutron cross sections exceed πR_p^2 is not so much due to $\lambda\!\!\!^{-}$ as to the fact that neutrons are strongly attracted to the nucleus. The expression $\pi(R+\lambda\!\!\!^{-})^2$ is apparently a convenient (but misleading) way to represent the effects of that attraction.

APPENDIX C: THE EFFECT OF AN ATTRACTIVE PION-NUCLEUS POTENTIAL ON THE CROSS SECTION

If one introduces into the wave mechanical exercises of Appendix B a real potential having the same radial shape as the imaginary one, the calculated reaction cross section is found to increase linearly with the well depth. At an incident pion energy of 100 MeV (for both Ca and Pb) the cross section increases by 2.6% for every 10 MeV of central well depth.

Calculations using classical trajectories give essentially the same result. Moreover there is a correspondence in the change in shapes of the classical and wave-mechanical transmission functions when one turns on an attractive potential. For the same potential change one finds that the increase of $b_{1/2}$, the classical impact parameter, matches that of the wave mechanical angular momemtum, $\hbar l_{1/2}$, where $b_{1/2}$ and $\hbar l_{1/2}$ are the values for which the transmission equals $\frac{1}{2}$. Since the classical increase in cross section is due entirely to refraction and the wave mechanical effect mimics it so closely, it too must be essentially a refractive effect rather than an effect due to the addition of $\lambda\!\!\!^{-}$ to the nuclear radius.

---

*Present address: California State University, Los Angeles, CA 90032.

†Present address: Lawrence Berkeley Laboratory, Berkeley, CA 94720.

‡Present address: Physics Department, University of New Mexico, Albuquerque, NM 87131.

§Present address: Physics Department, University of Pittsburgh, Pittsburgh, PA 15260.

**Present address: Nuclear Physics Laboratory, University of Illinois, Champaign, IL 61801.

††Present address: Physics Department, Princeton University, Princeton, NJ 08544.

‡‡Present address: Brookhaven National Laboratory, Upton, NY 11973.

§§Present address: Physics Department, Wheaton College, Wheaton, IL 60187.

[1]G. R. Burleson, G. S. Blanpied, J. Davis, J. S. McCarthy, R. C. Minehart, C. Goulding, C. L. Morris, H. A. Thiessen, W. B. Cottingame, S. Greene, and C. F. Moore, Phys. Rev. C **21**, 1452 (1980).

[2]J. Rohlin, S. Rohlin, B. W. Allardyce, J. J. Domingo, C. H. Q. Ingram, N. W. Tanner, E. M. Rimmer, and J. P. Girardeau-Montaut, Nucl. Phys. **B37**, 461 (1972).

[3]M. Blecher, K. Gotow, R. Ng, R. L. Burman, R. Carlini, S. Dam, M. V. Hynes, M. J. Leitch, V. Sandberg, R. Auble, F. E. Bertrand, E. E. Gross, F. E. Obenshain, J. Wu, G. S. Blanpied, B. M. Preedom, B. G. Ritchie, W. Bertozzi, M. A. Kovash, and R. P. Redwine, Phys. Rev. C **25**, 2554 (1982).

[4]R. D. McKeown, S. J. Sanders, J. P. Schiffer, H. E. Jackson, M. Paul, J. R. Specht, E. J. Stephenson, R. P. Redwine, and R. E. Segel, Phys. Rev. C **24**, 211 (1981).

[5]S. M. Levenson, D. F. Geesaman, E. P. Colton, R. J. Holt, H. E. Jackson, J. P. Schiffer, J. R. Specht, K. E. Stephenson, B. Zeidman, R. E. Segel, P. A. M. Gram, and C. A. Goulding, Phys. Rev. C **28**, 326 (1983).

[6]D. Ashery, I. Navon, G. Azuelos, H. K. Walter, H. J. Pfeiffer, and F. W. Schlepütz, Phys. Rev. C **23**, 2173 (1981).

[7]H. W. Bertini, Phys. Rev. **131**, 1801 (1963).

[8]R. R. Silbar, Phys. Rev. C **11**, 1610 (1975).

[9]C. H. Q. Ingram, *Meson-Nuclear Physics—1979 (Houston)*, Proceedings of the 2nd International Topical Conference on Meson-Nuclear Physics, AIP Conf. Proc. No. 54, edited by E. V. Hungerford (AIP, New York, 1979), p. 455.

[10]J. N. Ginocchio, Phys. Rev. C **17**, 195 (1978).

[11]J. P. Schiffer, Nucl. Phys. **A335**, 339 (1980).

[12]Z. Fraenkel, E. Piasetzky, and G. Kalbermann, Phys. Rev. C **26**, 1618 (1982).

[13]E. Piasetzky, R. R. Silbar, and M. M. Sternheim, Phys. Rev. C **25**, 2830 (1982); Y. Ohkubo and N. T. Porile, *ibid.* **25**, 2638 (1982); M. Thies, Swiss Institute of Nuclear Research Report PR79-007, 1979.

[14]P. Y. Bertin, B. Coupat, A. Hivernat, D. B. Isabelle, J. Duclos, A. Gerard, J. Miller, J. Morgenstern, J. Picard, P. Vernin, and R. Powers, Nucl. Phys. **B106**, 341 (1976).

[15]K. G. R. Doss, P. D. Barnes, N. Colella, S. A. Dytman, R. A. Eisenstein, C. Ellegaard, F. Takeutchi, W. R. Wharton, J. F. Amann, R. H. Pehl, and A. C. Thompson, Phys. Rev. C **25**, 962 (1982).

[16]G. Rowe, M. Salomon, and R. H. Landau, Phys. Rev. C **18**, 584 (1978).

[17]J. F. Amann, P. D. Barnes, K. G. R. Doss, S. A. Dytman, R. A. Eisenstein, J. D. Sherman, and W. R. Wharton, Phys. Rev. C **23**, 1635 (1981).

[18]M. Blecher, K. Gotow, R. L. Burman, M. V. Hynes, M. J. Leitch, N. S. Chant, L. Rees, P. G. Ross, F. E. Bertrand, E. E. Gross, F. E. Obenshain, T. P. Sjoreen, G. S. Blanpied, B. M. Preedom, and B. G. Ritchie, Phys. Rev. C **28**, 2033 (1983).

[19]C. H. Q. Ingram, P. A. M. Gram, J. Jansen, R. E. Mischke, J.

Zichy, J. Bolger, E. T. Boschitz, G. Probstle, and J. Arvieux, Phys. Rev. C **27**, 1578 (1983).

[20]B. J. Dropesky, G. W. Butler, C. J. Orth, R. A. Williams, M. A. Yates-Williams, G. Friedlander, and S. B. Kaufman, Phys. Rev. C **20**, 1844 (1979); B. J. Lieb, H. S. Plendl, C. E. Stronach, H. O. Funsten, and V. G. Lind, *ibid.* **19**, 2405 (1979).

[21]E. Piasetzky, D. Ashery, A. Altman, A. I. Yavin, F. W. Schlepütz, R. J. Powers, W. Bertl, L. Felawka, H. K. Walter, R. G. Winter, and J. v. d. Pluym, Phys. Rev. Lett. **46**, 1271 (1981); J. A. Faucett, B. E. Wood, D. K. McDaniels, P. A. M. Gram, M. E. Hamm, M. A. Oothoudt, C. A. Goulding, L. W. Swenson, K. S. Krane, A. W. Stetz, H. S. Plendl, J. Norton, H. Funsten, and D. Joyce, Phys. Rev. C **30**, 1622 (1984).

[22]R. E. Mischke, A. Blomberg, P. A. M. Gram, J. Jansen, J. Zichy, J. Bolger, E. Boschitz, C. H. Q. Ingram, and G. Pröbstle, Phys. Rev. Lett. **44**, 1197 (1980); S. A. Wood, J. L. Matthews, G. A. Rebka, P. A. M. Gram, H. J. Ziock, and D. A. Clark, *ibid.* **54**, 635 (1985).

[23]M. J. Jakobson, G. R. Burleson, J. R. Calarco, M. D. Cooper, D. C. Hagerman, I. Halpern, R. H. Jeppeson, K. F. Johnson, L. D. Knutson, R. E. Marrs, H. O. Meyer, and R. P. Redwine, Phys. Rev. Lett. **38**, 1201 (1977).

[24]C. W. de Jager, H. de Vries, and C. de Vries, At. Data Nucl. Data Tables **14**, 479 (1974).

[25]S. B. Kaufman, E. P. Steinberg, and G. W. Butler, Phys. Rev. C **20**, 2293 (1979).

[26]E. Friedman, Phys. Rev. C **28**, 1264 (1983).

[27]K. Stricker, H. McManus, and J. A. Carr, Phys. Rev. C **19**, 929 (1979).

[28]D. Ashery, D. F. Geesaman, R. J. Holt, H. E. Jackson, J. R. Specht, K. E. Stephenson, R. E. Segel, P. Zupranski, H. W. Baer, J. D. Bowman, M. D. Cooper, M. Leitch, A. Erel, J. Comuzzi, R. P. Redwine, and D. R. Tieger, Phys. Rev. C **30**, 946 (1984).

[29]E. Piasetzky, A. Altman, J. Lichtenstadt, A. I. Yavin, D. Ashery, W. Bertl, L. Felawka, H. K. Walter, F. W. Schlepütz, R. J. Powers, R. G. Winter, and J. v. d. Pluym, Phys. Lett. B **114**, 414 (1982); E. Piasetzky, Phys. Rev. C **27**, 773 (1983).

[30]K. G. R. Doss *et al.* (unpublished).

[31]D. Chiang, Ph.D. thesis, University of Washington, 1980 (unpublished).